XII Congreso Argentino de Seguridad Radiológica y Nuclear

3 y 4 de septiembre de 2019

Centro Atómico Constituyentes - CNEA

Radiaciones No Ionizantes desde λ = 300 nm hasta 3 mm. Caracterización. Protección. Advertencias.

Mario Garavaglia.

Departamento de Física, Universidad Nacional de La Plata y Centro de Investigaciones Ópticas (CIOp). La Plata.

garavagliam@ciop.unlp.edu.ar

S.A.R.

SOCIEDAD ARGENTINA DE RADIOPROTECCION

¡Agradezco la invitación a participar de esta sesión RNI!

ESPECTRO ELECTROMAGNÉTICO I

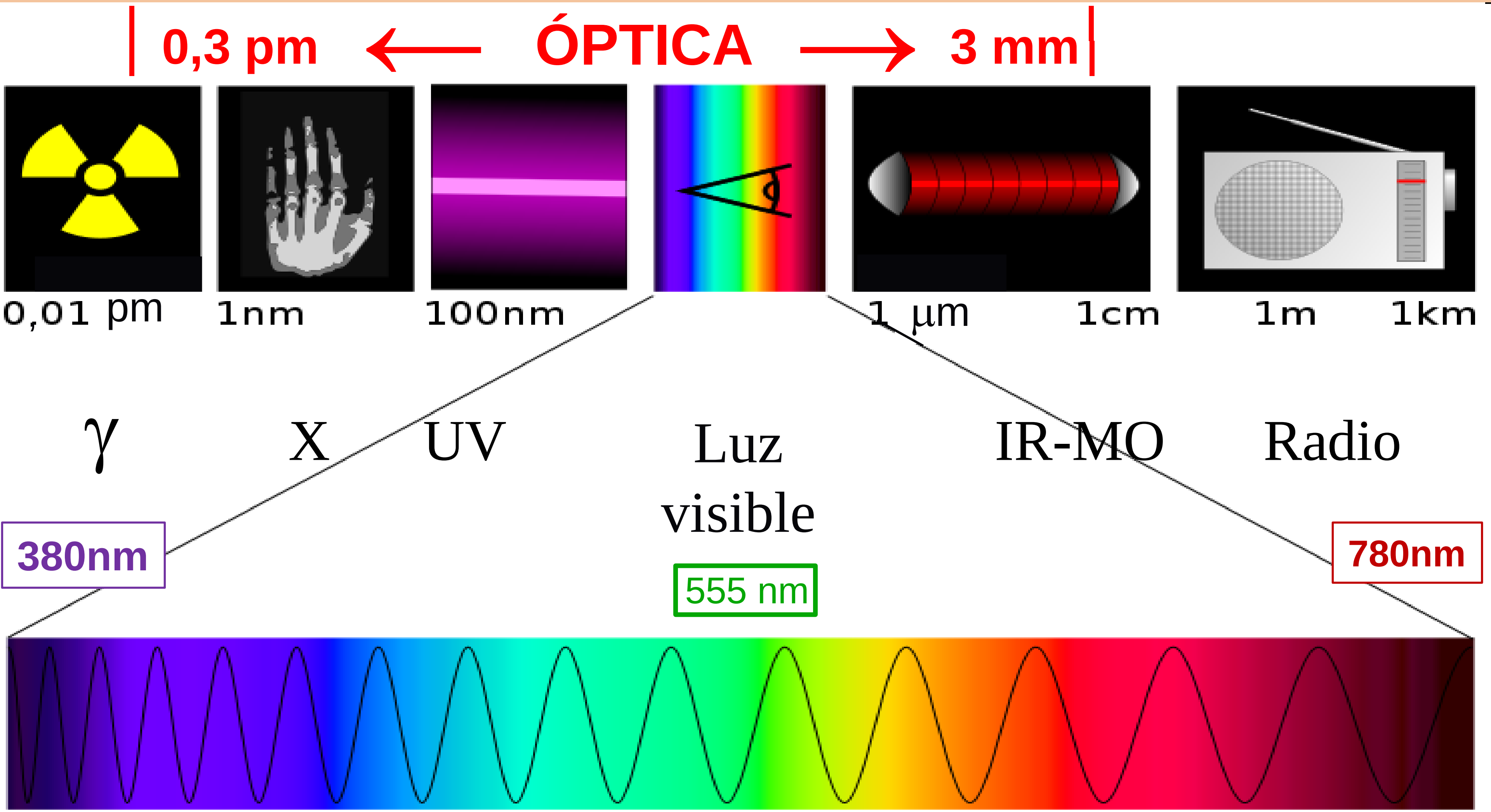

ESPECTRO ELECTROMAGNÉTICO II

Totalmente Invasivo

No Invasivo, pero ¡cuidado!

No Invasivo

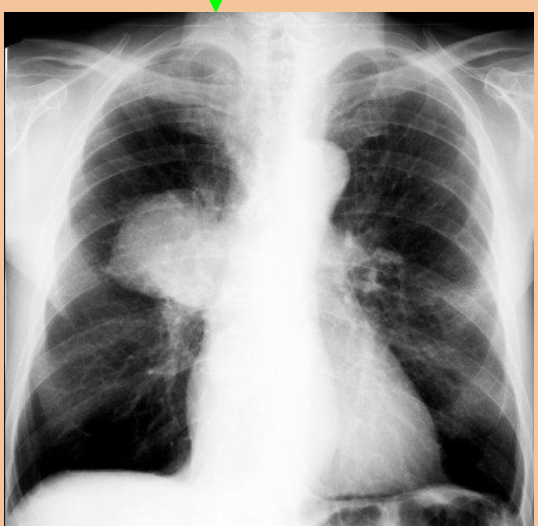

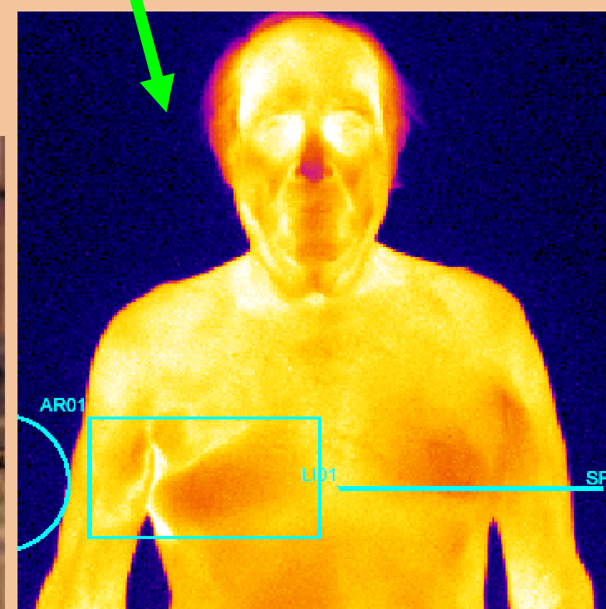

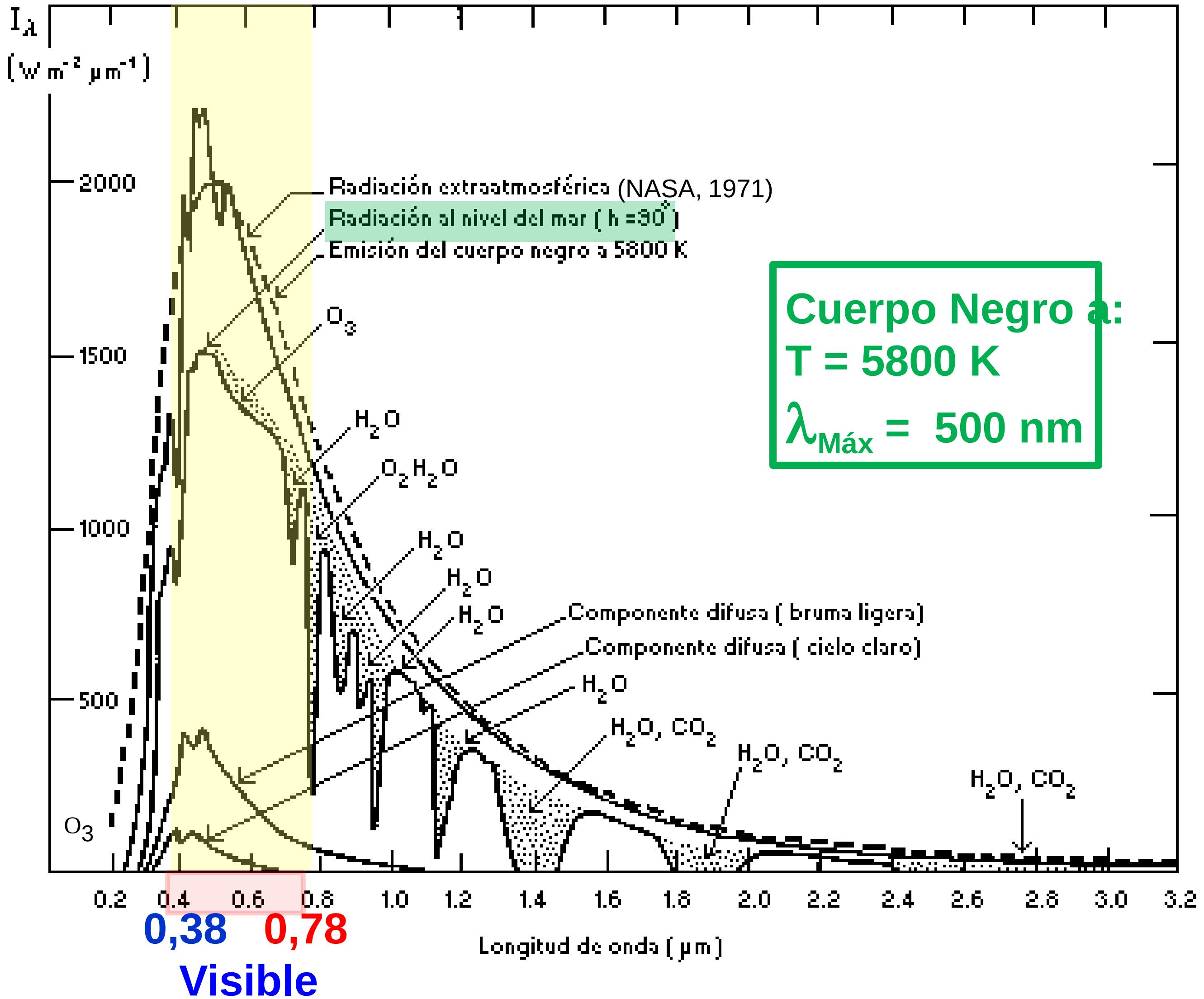

Distribución espectral de la radiación solar que incide perpendicularmente sobre la atmósfera terrestre y su valor a nivel del mar. (según Chassériaux, 1990)

CONTRIBUCIÓN DEL LABORATORIO DE ACÚSTICA Y LUMINOTECNIA (LAL-CIC) I

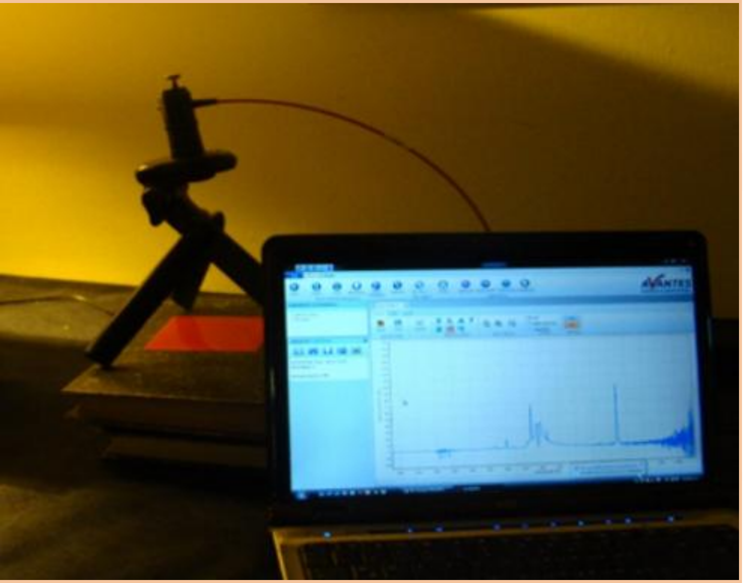

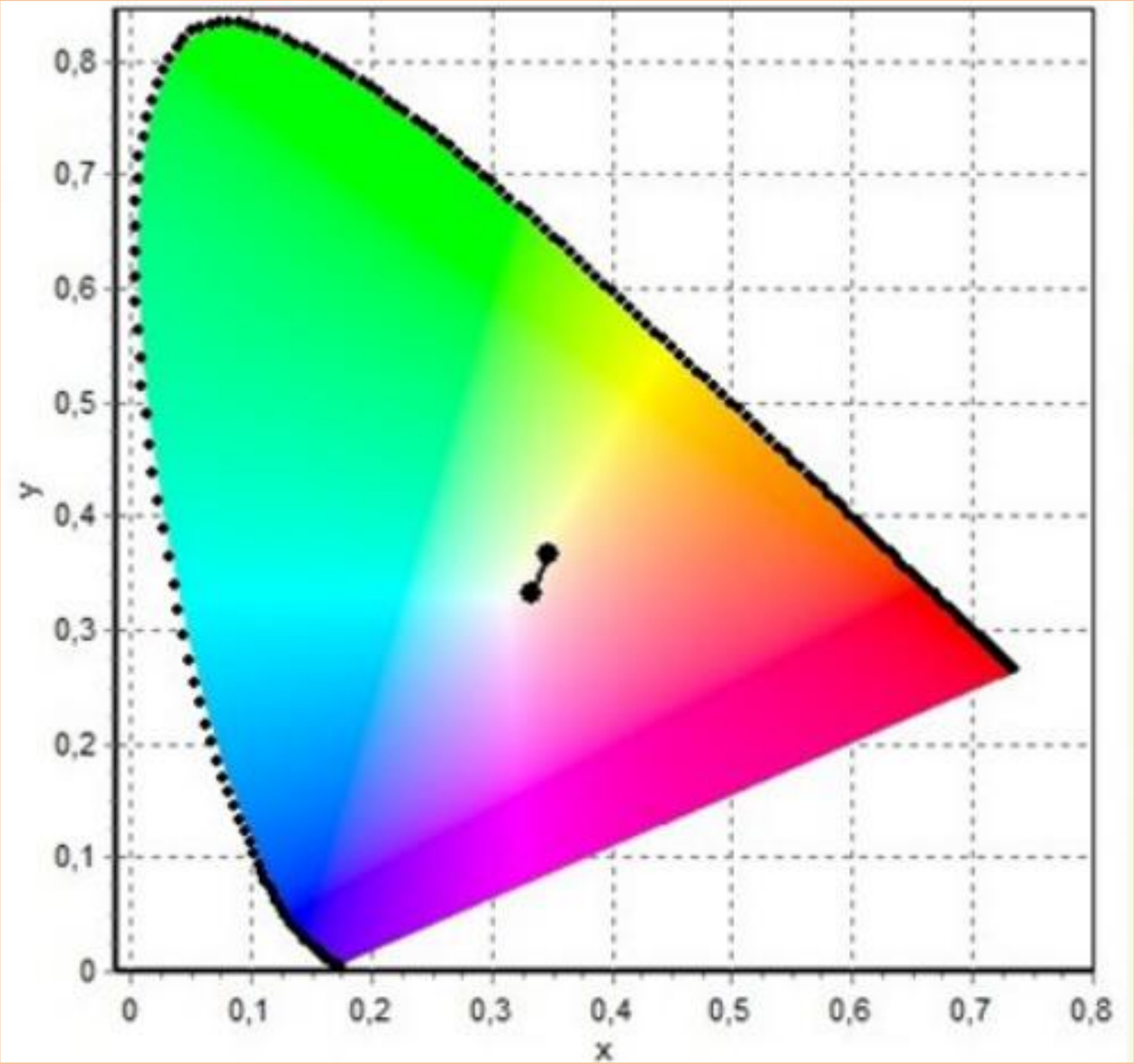

Agradezco al Prof. Ing. Pablo Ixtaina, Director del LAL.

CONTRIBUCIÓN DEL LABORATORIO DE ACÚSTICA Y LUMINOTECNIA (LAL-CIC) II

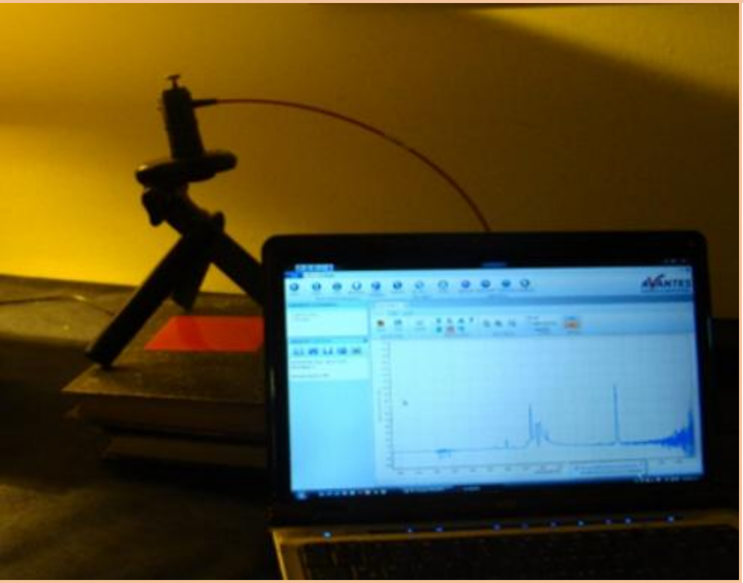

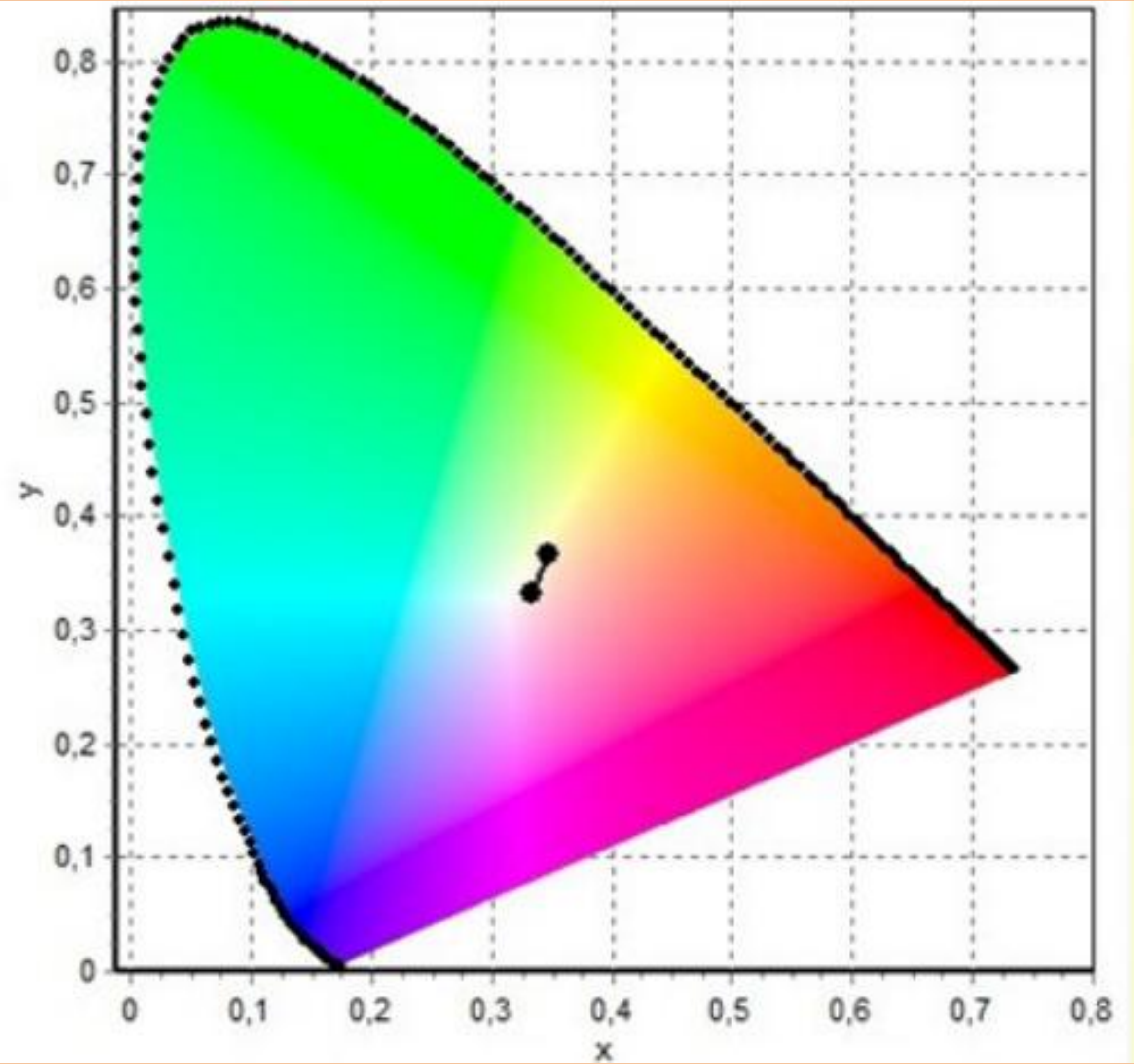

Agradezco al Prof. Ing. Pablo Ixtaina, Director del LAL.

PREMIO NOBEL DE FISICA 2014

Isamu Akasaki (1929) Hiroshi Amano (1960) Shüji Nakamura (1954)

Inventores del diodo emisor de luz LED y LD azul,
"una nueva luz para iluminar el mundo“ [⅓Parte c/u]

PREMIO NOBEL DE FISICA 2014

Shūji Nakamura
(1954 -) [⅓Parte]

«por la invención de eficientes diodos de emisión de luz azules, que han hecho posibles las fuentes de luz blanca brillantes y de bajo consumo»

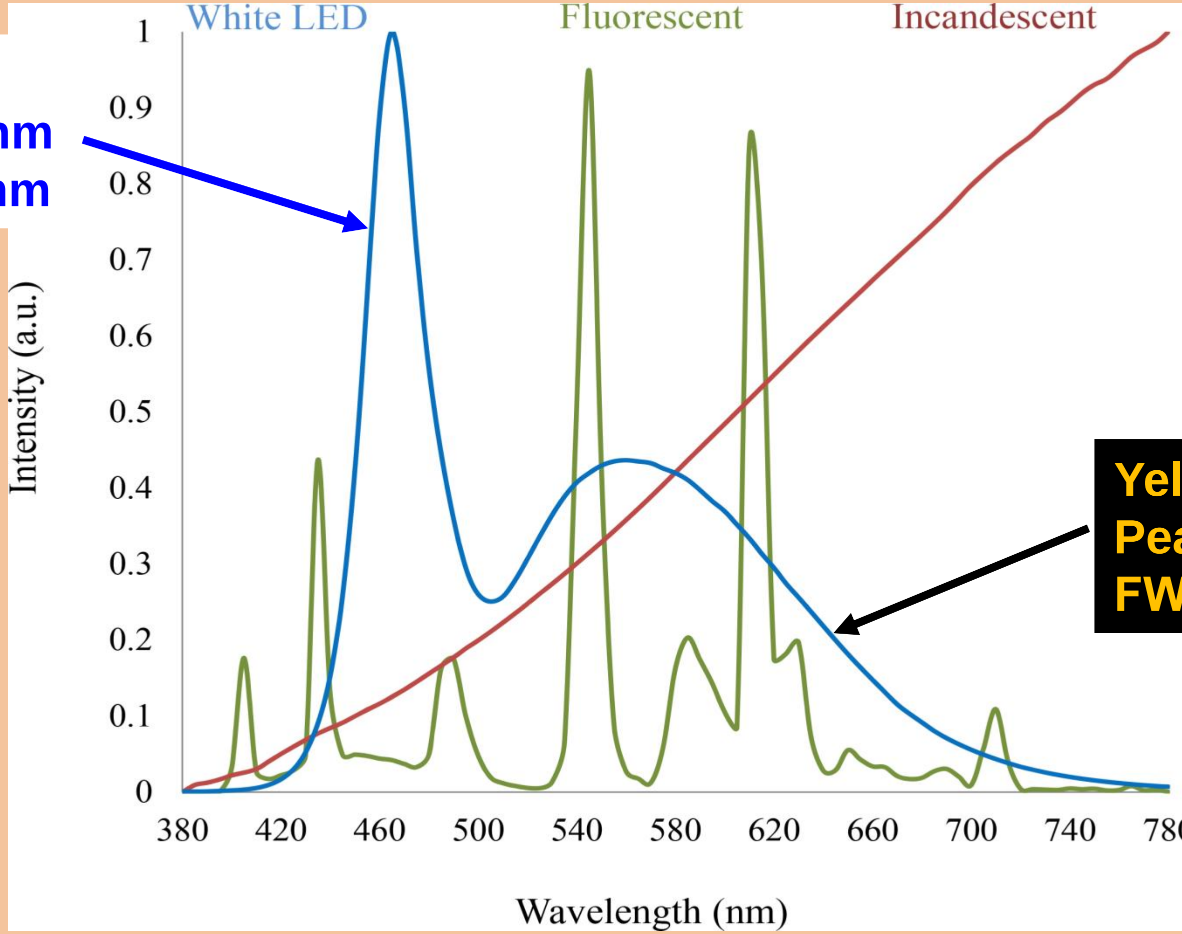

A comparison of the power spectrum of a standard white-light LED, a tricolor fluorescent lamp, and an incandescent source. The radically different power spectrums can look similar when viewed directly by the eye, irrespective of how much blue emission is present.

EFFECTS OF BLUE LIGHT ON THE CIRCADIAN SYSTEM AND EYE PHYSIOLOGY
Gianluca Tosini, Ian Ferguson, and Kazuo Tsubota
Molecular Vision 2016; 22:61-72 <http://www.molvis.org/molvis/v22/61>

TRANSMISIÓN DE LUZ EN EL OJO

Como para bebés, niños y adolescentes

Como a partir de los 25 años

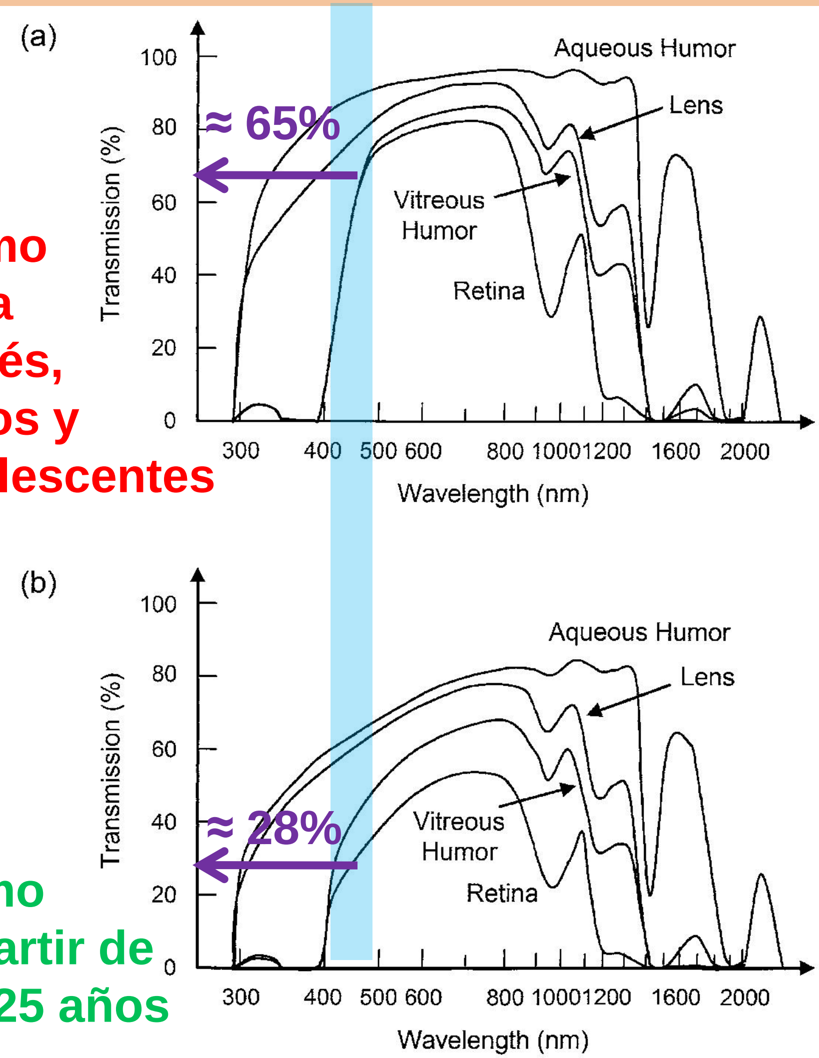

Fig. 11.18. Transmission of near-ultraviolet, visible, and near-infrared light through the eye up to the labeled part of the eye. In (**a**) only transmission losses due to absorption are included, while in (**b**) all transmission losses are accounted for, including those due to absorption and scattering. (Based on [514] and [527])

$$R=\left(\frac{n_2-n_1}{n_2+n_1}\right)^2$$

Ley de Fresnel

$$I(z)=I(z=0)\exp\left(-\alpha_{Absorción}z\right)$$

Ley de Beer

$$I(z)=I(z=0)\exp\left(-\alpha_{Scattering}z\right)$$

$$\alpha_{Scattering}=\frac{8\pi^4}{3}\frac{ND^4}{\lambda^4}\left(\frac{n_p^2-n_a^2}{n_p^2+2n_a^2}\right)^2$$

Scattering Rayleigh: N es la concentración de partículas de diámetro D e índice de refracción n_p.

ESPECTRO ELECTROMAGNÉTICO III

Velocidad de la luz en el vacío

$$c = \nu \times \lambda$$

c = *299 792 458 m/s*

Energía de un fotón

$$E_\nu = h \times \nu$$

Constante de Planck

$h \approx 6{,}62607 \times 10^{-34}$ Js

El dígito 7 acumula las aproximaciones de los siguientes: 7 = 6983.

(XXVI CGPM, 13-16/11/2018)

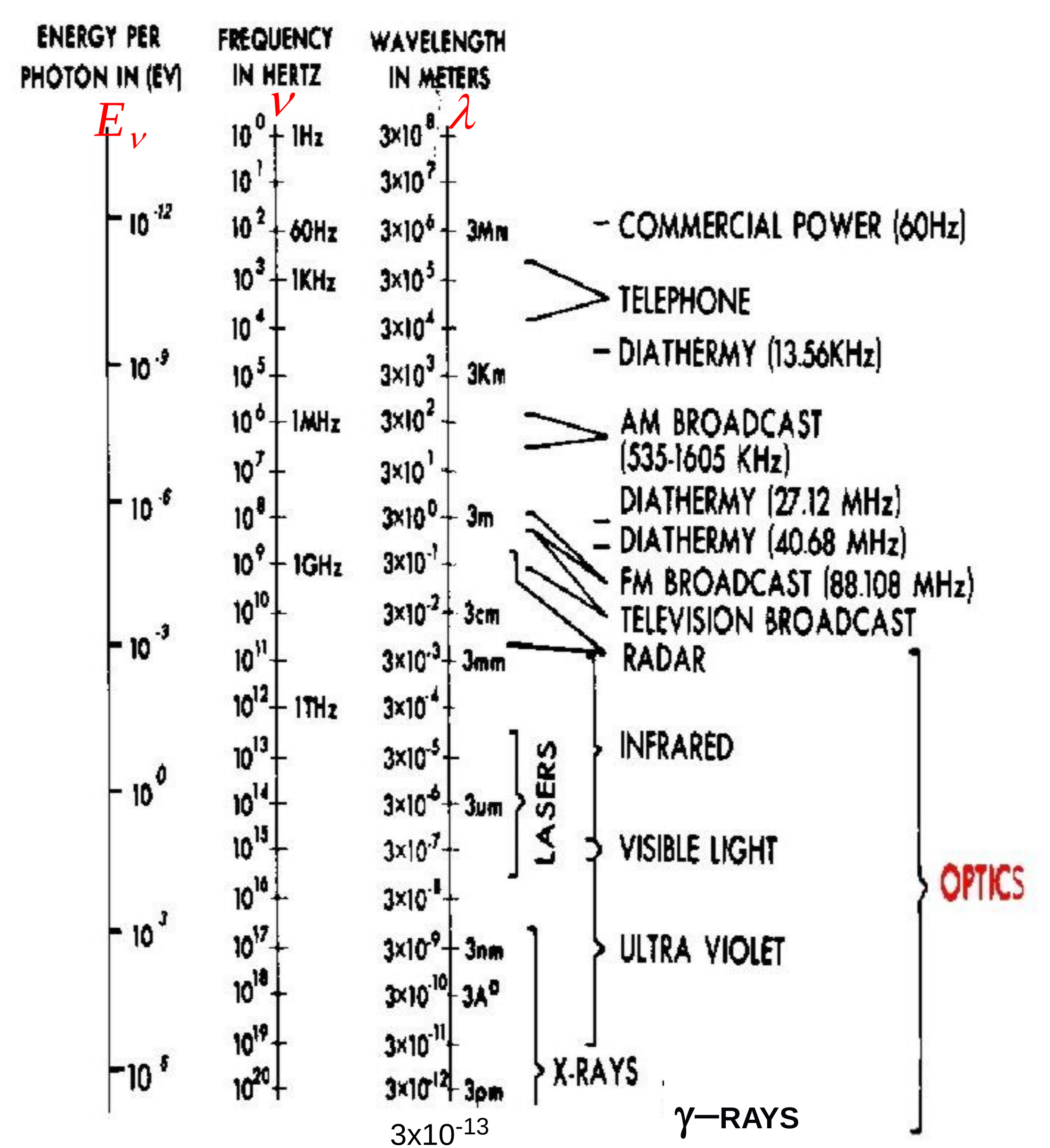

EFECTOS PRODUCIDOS EN LA INTERACCIÓN LÁSER-TEJIDOS

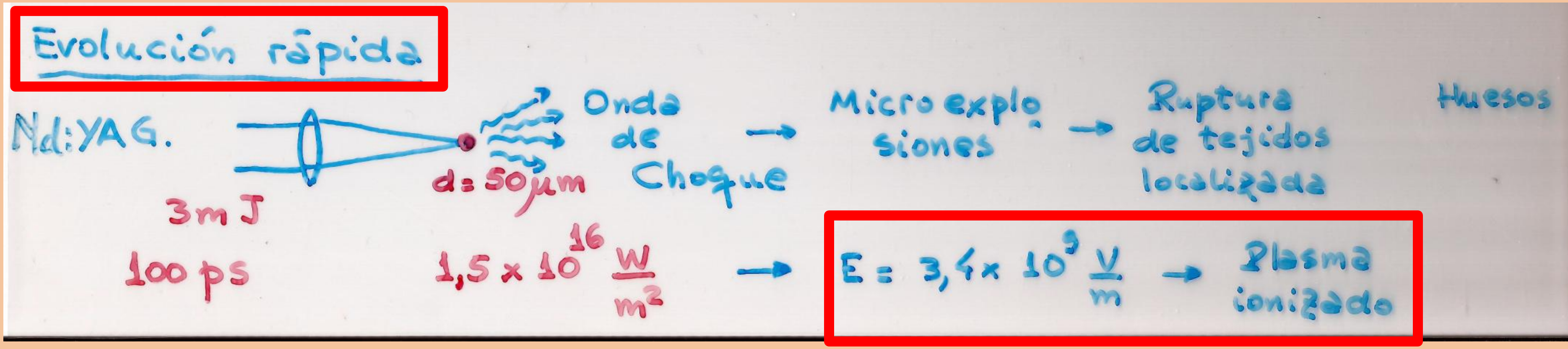

$$I = P/A = 1{,}53\times 10^{16}\, W/m^2$$

$$I = \frac{c\varepsilon_0}{2} E^2$$

$$E = \sqrt{\frac{2I}{c\varepsilon_0}} = \sqrt{\frac{2\times 1{,}53\times 10^{16}\, W/m^2}{3\times 10^8\,(m/s)\times 8{,}85\times 10^{-12}\,(s^2C^2/m^3kg)}} \approx$$

$$E \approx 3{,}4\times 10^9\,\frac{V}{m}$$

¿Dejamos a los láseres entre las fuentes de RNI?

AUTOPROTECCIÓN DEL OJO AL UV

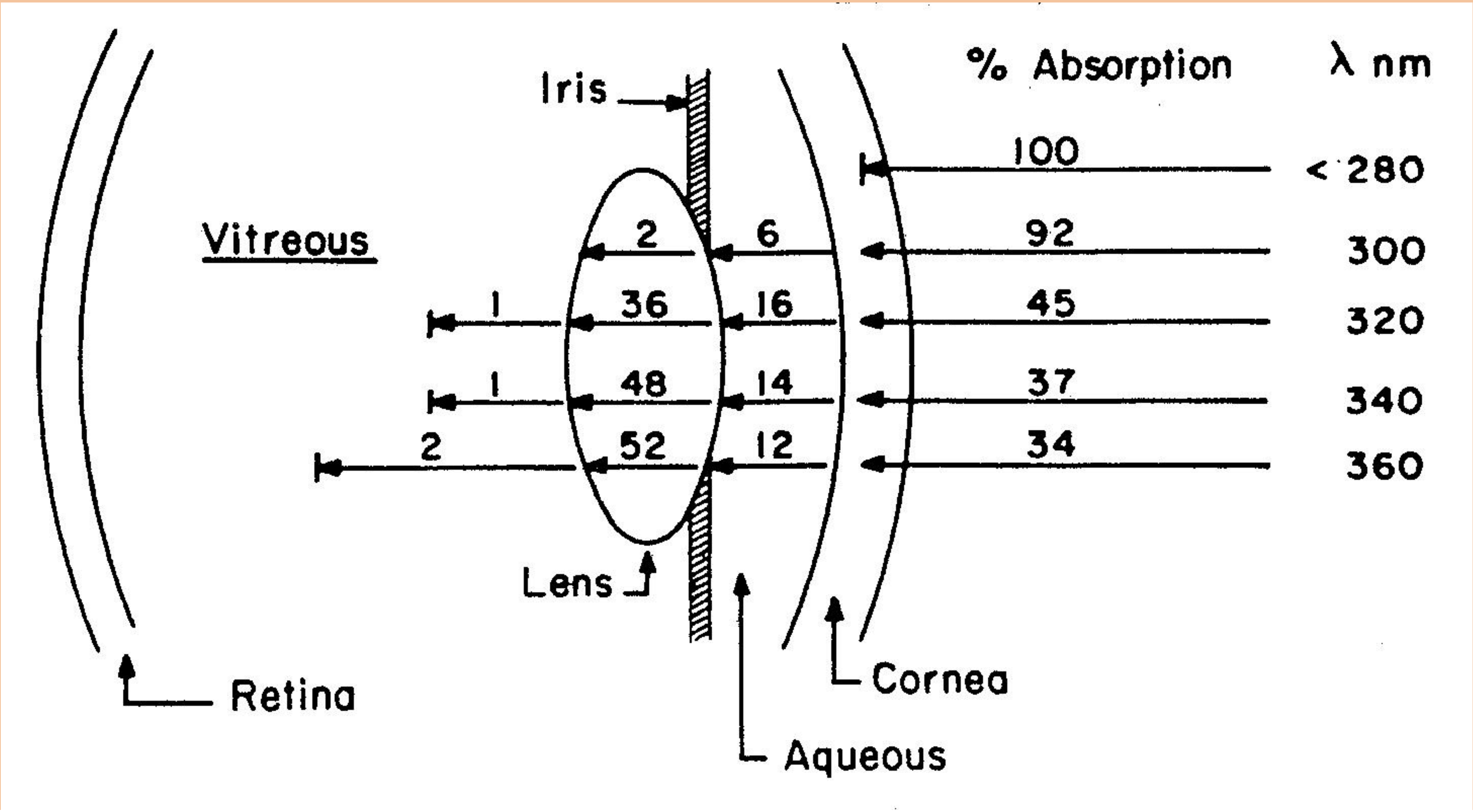

El espectro ultravioleta (UV) varía entre 100 y 400 nm y se subdivide en cuatro bandas: la región del Vacío (100 a 200 nm), la región UVC (200 a 280 nm), la región UVB (280 a 315 nm) y la región UVA (315 a 400 nm)

DAÑO EN RETINA DE CODORNIZ POR LÁSER DE ARGÓN EN λ = 488 nm.

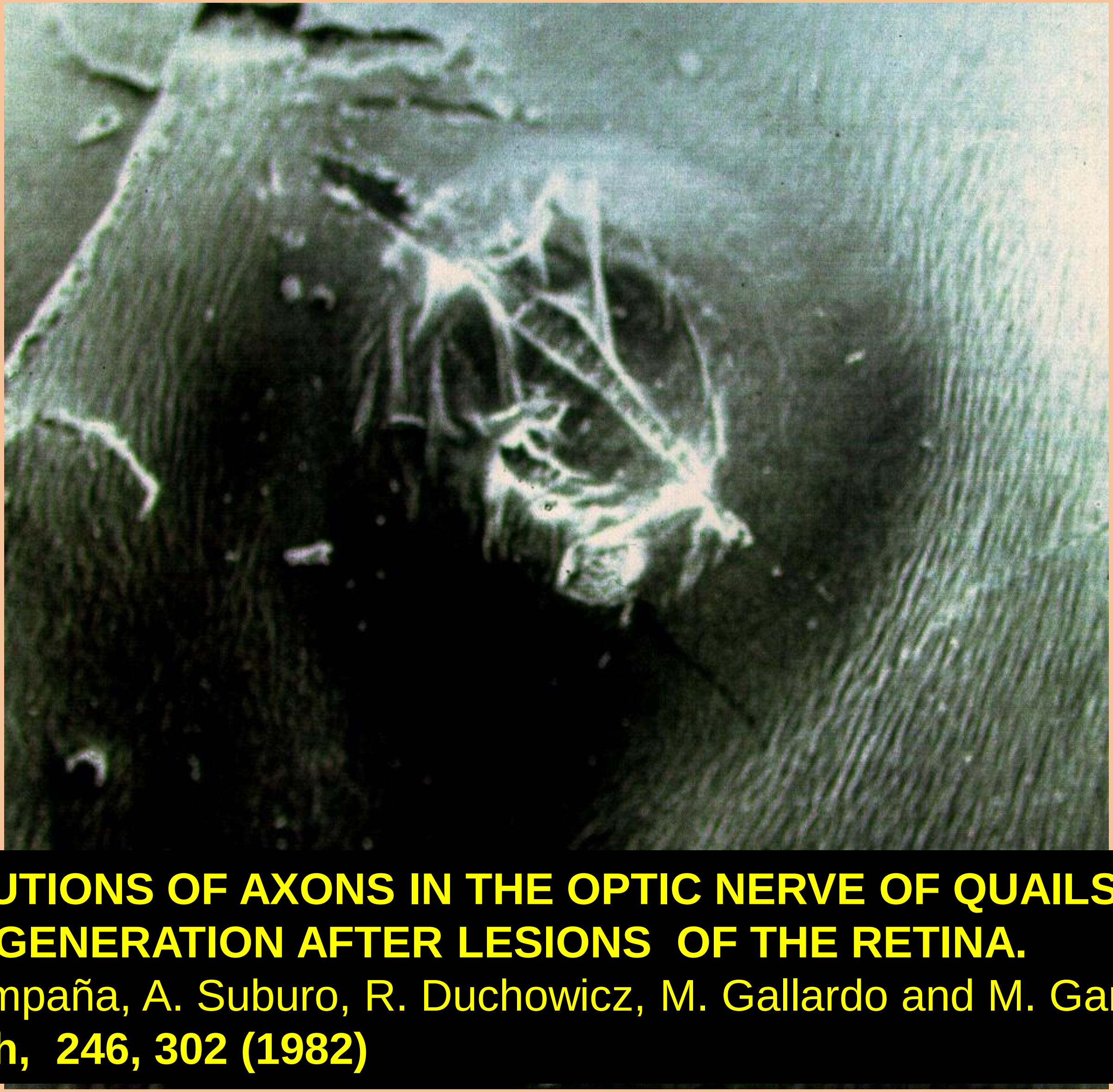

TWO DISTRIBUTIONS OF AXONS IN THE OPTIC NERVE OF QUAILS: A STUDY OF NERVE DEGENERATION AFTER LESIONS OF THE RETINA.

N. Carri, H. Campaña, A. Suburo, R. Duchowicz, M. Gallardo and M. Garavaglia

Brain Research, 246, 302 (1982)

ICNIRP GUIDELINES

ON LIMITS OF EXPOSURE TO LASER RADIATION OF WAVELENGTHS BETWEEN 180 nm AND 1,000 µm

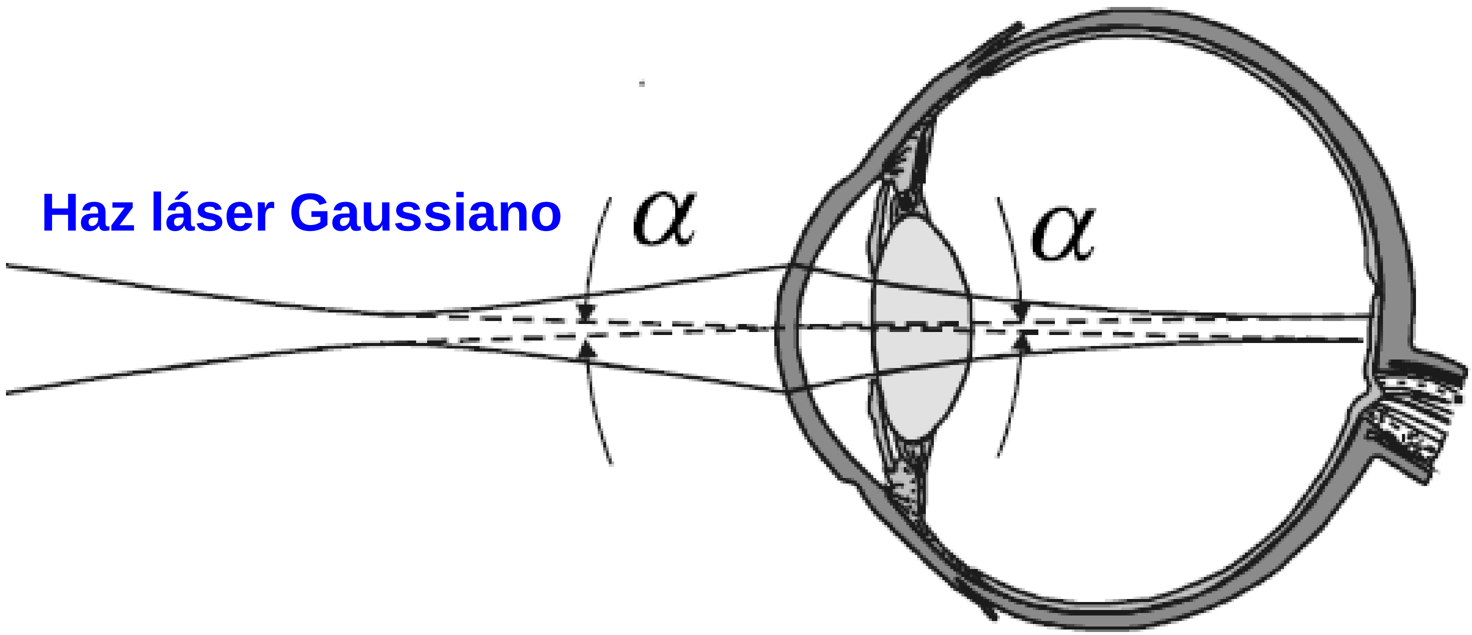

Fig. 3. The parameter α, for a given position of the eye in the beam is the angle subtended by the apparent source that produces the minimal retinal beam profile that can be achieved by accommodation of the eye. The figure is simplified assuming an air-filled eye and that the eye can accommodate to a distance very close to the eye.

Resolución 295-03 Láser (10/10/2016)

Ministerio de Trabajo, Empleo y Seguridad Social, Argentina.

TABLA 1

Aberturas límites aplicables a los TLVs del láser

Región Espectral	Duración	Ojo	Piel
180 nm - 400 nm	1 ns a 0,25 s	1 mm	3,5 mm
180 nm - 400 nm	0,25 s a 30 ks	3,5 mm	3,5 mm
* 400 nm - 1400 nm	10^{-4} ns a 0,25 s	7 mm	3,5 mm
400 nm - 1400 nm	0,25 s a 30 ks	7 mm	3,5 mm
*1400 nm - 0,1 mm	10^{-5} ns a 0,25 s	1 mm	3,5 mm
1400 nm - 0,1 mm	0,25 s a 30 ks	3,5 mm	3,5 mm
* 0,1 mm - 1,0 mm	10^{-5} ns a 30 ks	11 mm	11 mm

Tamaño de la fuente y factor de corrección C_E

Para la duración de la exposición "t", el ángulo $\alpha_{mín}$ se define como:

$\alpha_{mín}$ = 1,5 mrad para t < 0,7 segundos (s).

Además, el factor corrector $C_E = 1$.

Para la duración de la exposición "t", el ángulo $\alpha_{mín}$ se define como:

$\alpha_{mín}$ = 1,5 mrad para t < 0,7 segundos (s).

Además, el factor corrector $C_E = 1$.

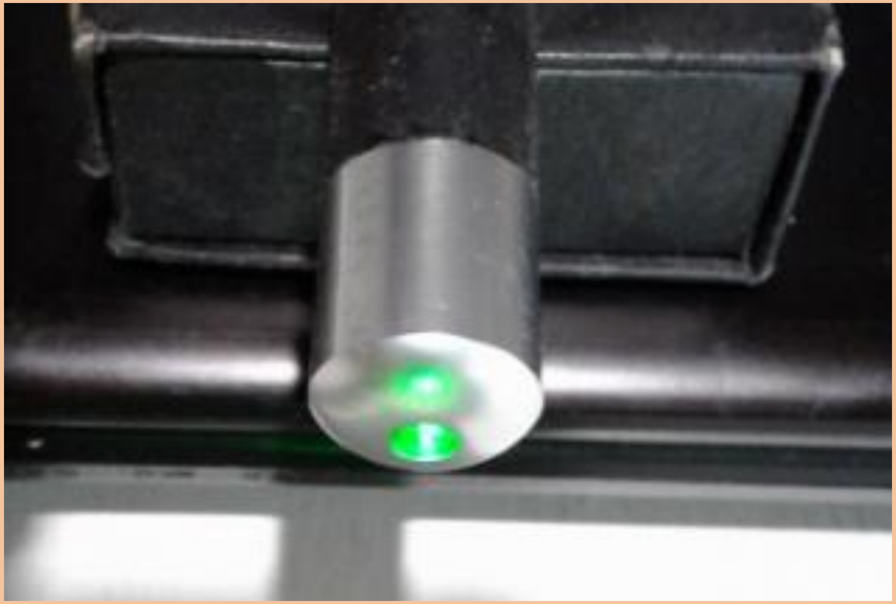

$Ø_{Haz\ láser}$ = 2 mm

$\alpha_{mín}$ = 1,5 mrad = 2 mm / L

L = 1,33 m

PUNTERO LÁSER (λ=532 nm, P=19 mW)

Mediciones realizadas en el CIOp

LINTERNA LÁSER (λ=650 nm, P=30 μW) I

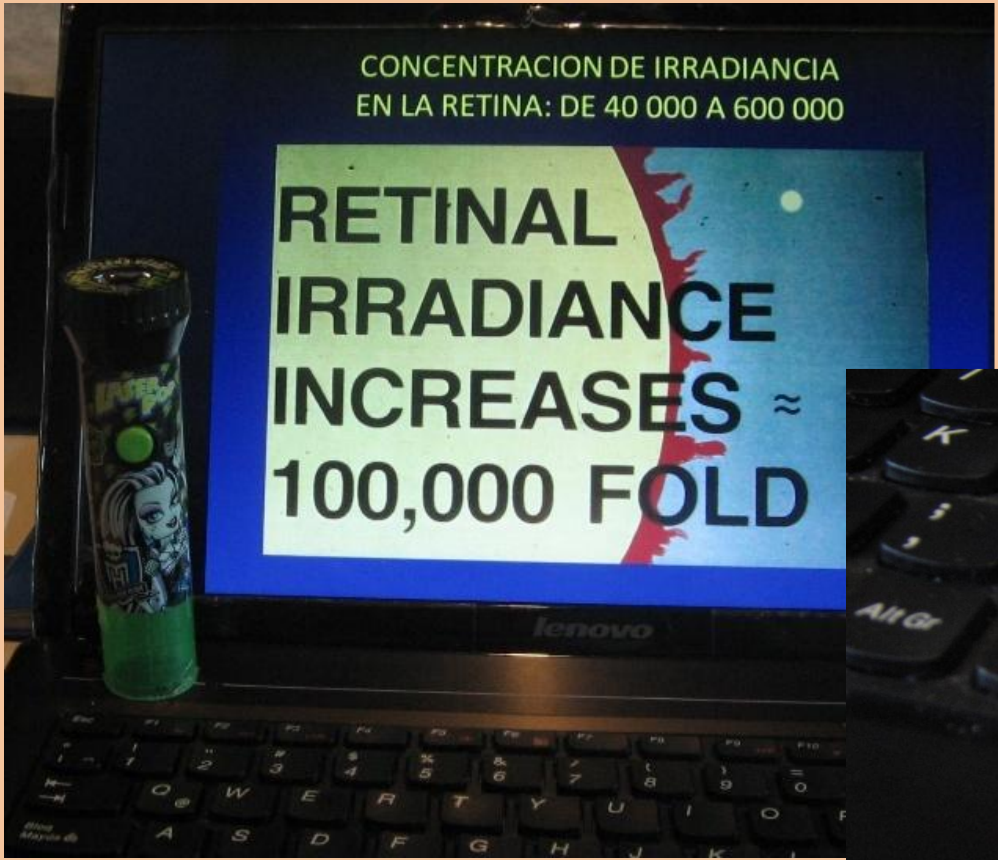

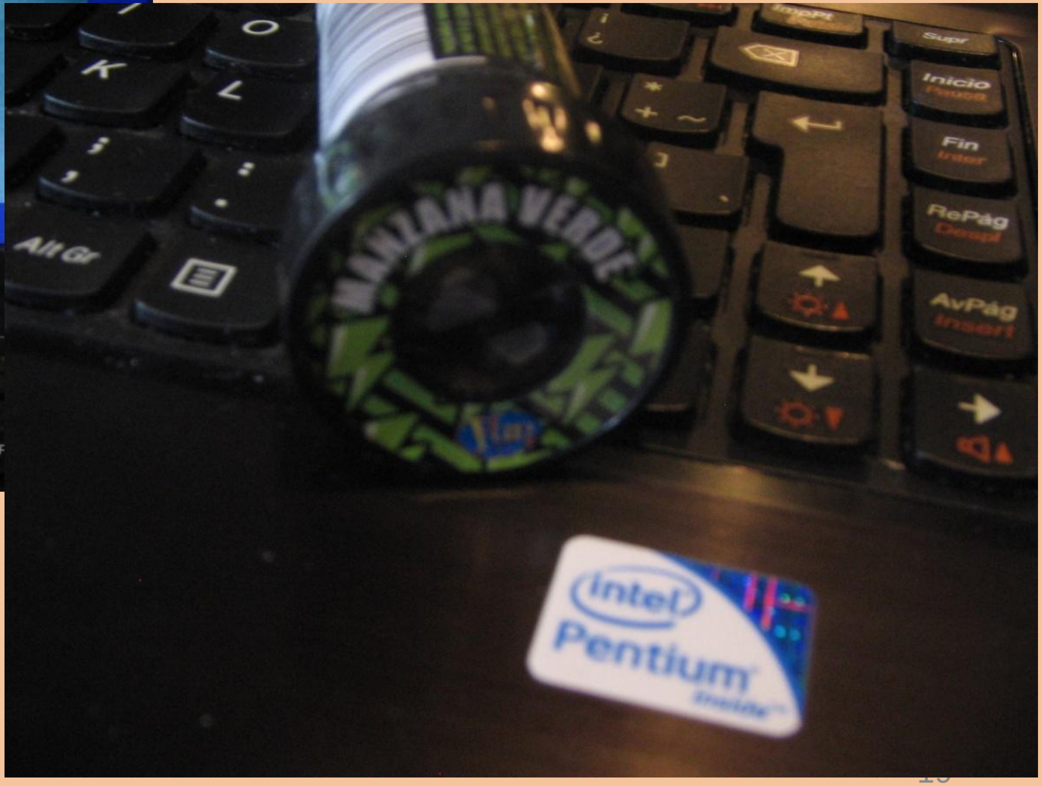

Mediciones realizadas en el CIOp

LINTERNA LÁSER (λ=650 nm, P=30 μW) II

TRANSMISIÓN DE LUZ EN EL OJO

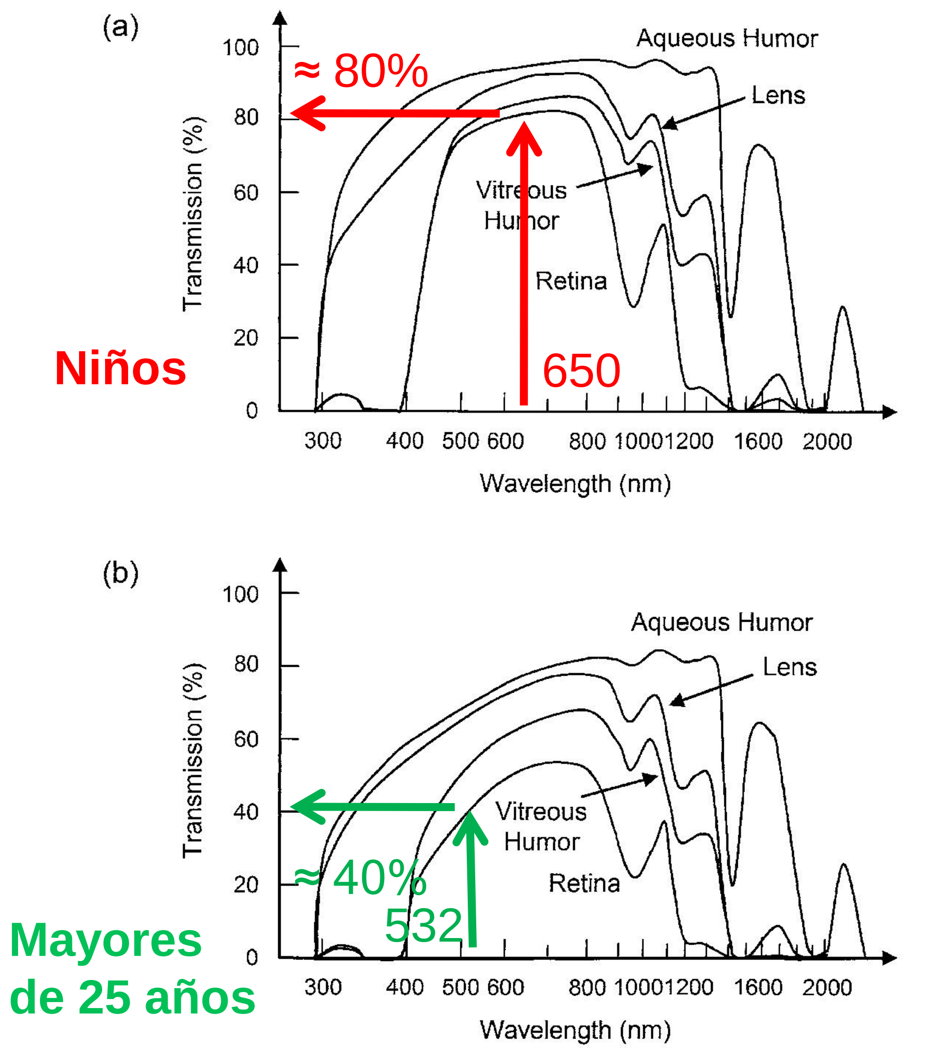

Fig. 11.18. Transmission of near-ultraviolet, visible, and near-infrared light through the eye up to the labeled part of the eye. In (**a**) only transmission losses due to absorption are included, while in (**b**) all transmission losses are accounted for, including those due to absorption and scattering. (Based on [514] and [527])

$$R = \left(\frac{n_2 - n_1}{n_2 + n_1} \right)^2$$

Ley de Fresnel

$$I(z) = I(z=0)\exp\left(-\alpha_{Absorción} z\right)$$

Ley de Beer

$$I(z) = I(z=0)\exp\left(-\alpha_{Scattering} z\right)$$

$$\alpha_{Scattering} = \frac{8\pi^4}{3} \frac{ND^4}{\lambda^4} \left(\frac{n_p^2 - n_a^2}{n_p^2 + 2n_a^2} \right)^2$$

Scattering Rayleigh: N es la concentración de partículas de diámetro D e índice de refracción n_p.

Irradiancia absorbida por la retina.
1: 2,4 kW/cm^2

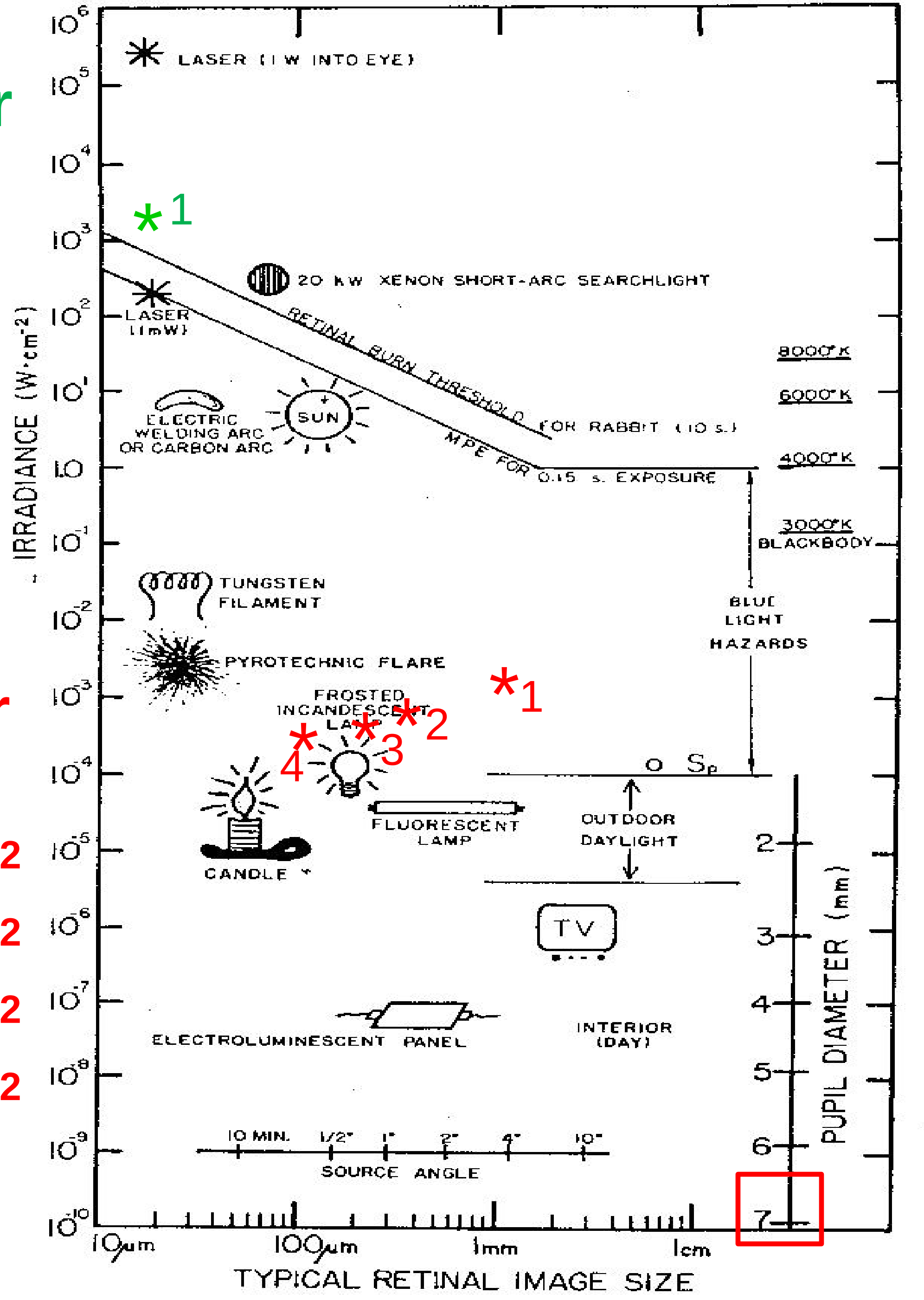

Distancia del puntero verde a la córnea: D=10 a 200 cm, y diámetro del spot del láser: d= 2 a 7 mm.

Irradiancia absorbida por la retina.
1: 1,05 mW/cm^2
2: 0,81 mW/cm^2
3: 0,63 mW/cm^2
4: 0,53 mW/cm^2

D: Distancia de la fuente a la córnea.
1: D=10 cm
2: D=30 cm
3: D=50 cm
4: D=100 cm

IRRADIANCIAS RETINIANAS

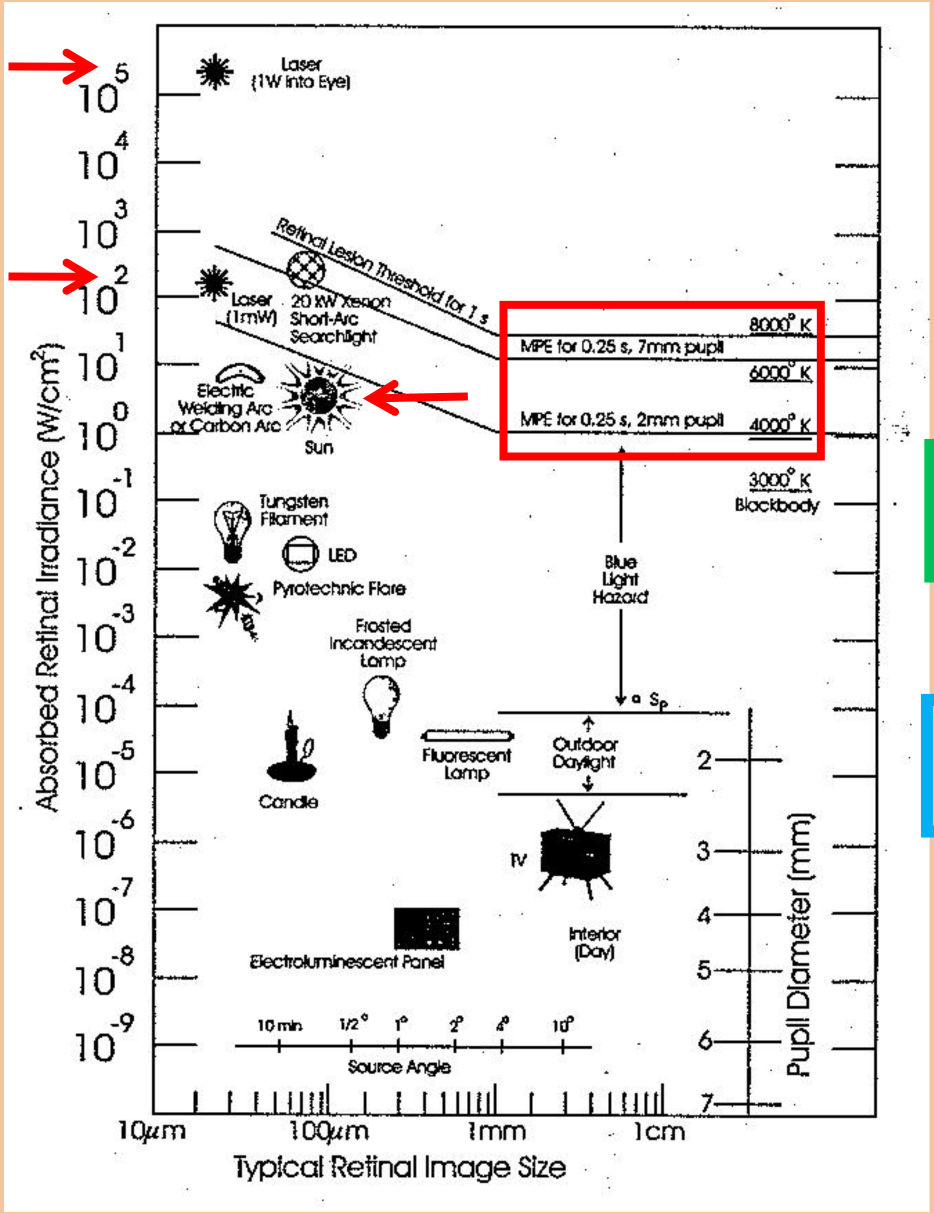

La absorción de luz depende del tiempo involucrado en el proceso. En la retina compiten varios:

- **-Fotoquímico**
  t > 10 s
- **-Coagulación térmica**
  10 ms < t < 10 s
- **-Termoacústico**
  t ≈ 1 a 5 ps
- **-Efectos no lineales**
  1 fs < t < 1 ps

$1\mu = 10^{-6}$
$1p = 10^{-12}$
$1f = 10^{-15}$

MPE ≡ Exposición Máxima Permitida

INTERACCIÓN LÁSER-TEJIDOS DEPENDE DE LA TASA DE EXPOSICIÓN Y LOS TIEMPOS DE INTERACCIÓN

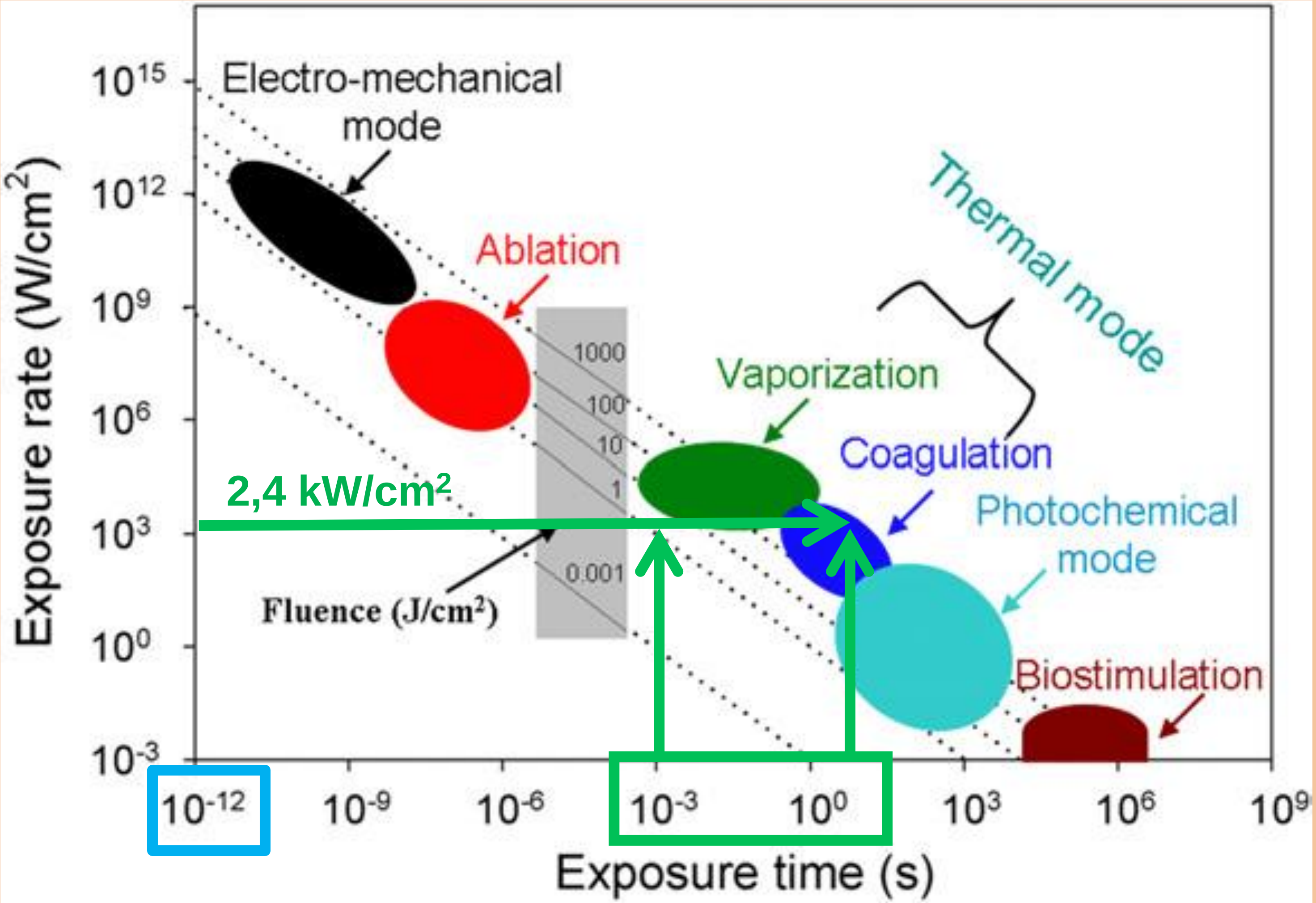

Resolución 295-03 Láser (10/10/2016)

Ministerio de Trabajo, Empleo y Seguridad Social, Argentina.

TABLA 2

Valores limite para exposiciones oculares directas (observación del interior del haz) a los rayos láser

Región del espectro	Longitud de onda	Tiempo de exposición (t) segundos	Valor límite
Luz visible	de 400 nm a 700 nm	de 10^{-13} a 10^{-11}	$1,5 \times 10^{-8}$ J/cm²
	de 400 nm a 700 nm	de 10^{-11} a 10^{-9}	$2,7(t/\sqrt[4]{t})$ J/cm²
	de 400 nm a 700 nm	de 10^{-9} a $1,8 \times 10^{-5}$	5×10^{-7} J/cm²
	de 400 nm a 700 nm	de $1,8 \times 10^{-5}$ a 10	$1,8\ (t/\sqrt[4]{t})$m J/cm²
10^4 s = 2,8 h	de 400 nm a 549 nm	de 10 a 10^4	10 m J/cm²
	de 550 nm a 700 nm	de 10 a T_1	$1,8\ (t/\sqrt[4]{t})$m J/cm²
	de 550 nm a 700 nm	de T_1 a 10^4	$10\ C_B$ mJ/cm²
	de 400 nm a 700 nm	de 10^4 a 3×10^4	$C_B\mu$ W/cm²

Valor límite para el puntero láser: 10 mJ/cm²

Valor límite para la linterna láser: 263,25 mJ/cm²

Resolución 295-03 Láser (10/10/2016)

Ministerio de Trabajo, Empleo y Seguridad Social, Argentina.

TABLA 2

Valores limite para exposiciones oculares directas (observación del interior del haz) a los rayos láser

Región del espectro	Longitud de onda	Tiempo de exposición (t) segundos	Valor límite
IRA	de 700 nm a 1049 nm	de 10^{-13} a 10^{-11}	1,5 C_A x 10^{-8} J/cm²
	de 700 nm a 1049 nm	de 10^{-11} a 10^{-9}	2,7 C_A $(t/\sqrt[4]{t})$ J/cm²
	de 700 nm a 1049 nm	de 10^{-9} a 1,8 x 10^{-5}	5 C_A x 10^{-7} J/cm²
	de 700 nm a 1049 nm	de 1,8 x 10^{-5} a 10^{3}	1,8 C_A $(t/\sqrt[4]{t})$ mJ/cm²

Valor límite para el láser analizado: 263,25 mJ/cm²

DENSIDAD ÓPTICA (OD en inglés)

Modo de expresión de la capacidad de absorción de un filtro, como las gafas protectoras para los usuarios de láseres. La **densidad óptica** (**DO**) se define como $\mathbf{DO = -\log_{10}(I_0/I)}$, siendo $\mathbf{I_0}$ la intensidad de la luz incidente sobre el filtro e **I** es la intensidad de la luz emergente del filtro. La transmitancia se define como $T = I/I_0$. Así, $T = 1 \rightarrow DO = 0$; $T = 0{,}32 \rightarrow DO = 0{,}5$;
$T = 0{,}1 = 10^{-1} \rightarrow DO = 1$; $T = 0{,}01 = 10^{-2} \rightarrow DO = 2$;
$T = 0{,}001 = 10^{-3} \rightarrow DO = 3$;
$T = 0{,}0001 = 10^{-4} \rightarrow DO = 4$;
$\mathbf{T = 0{,}00001 = 10^{-5} \rightarrow DO = 5}$.

GAFA PROTECTORA PARA LUZ LÁSER (780-830 nm, OD > 5)

Si DO > 5 → T < 0,000 001, lo que significa, matemáticamente, que de **algo más de 1 000 000 fotones** incidentes sobre la gafa no pasará **ninguno**.

PROTECTORES VISUALES
Y ACCIDENTE POR LÁSER

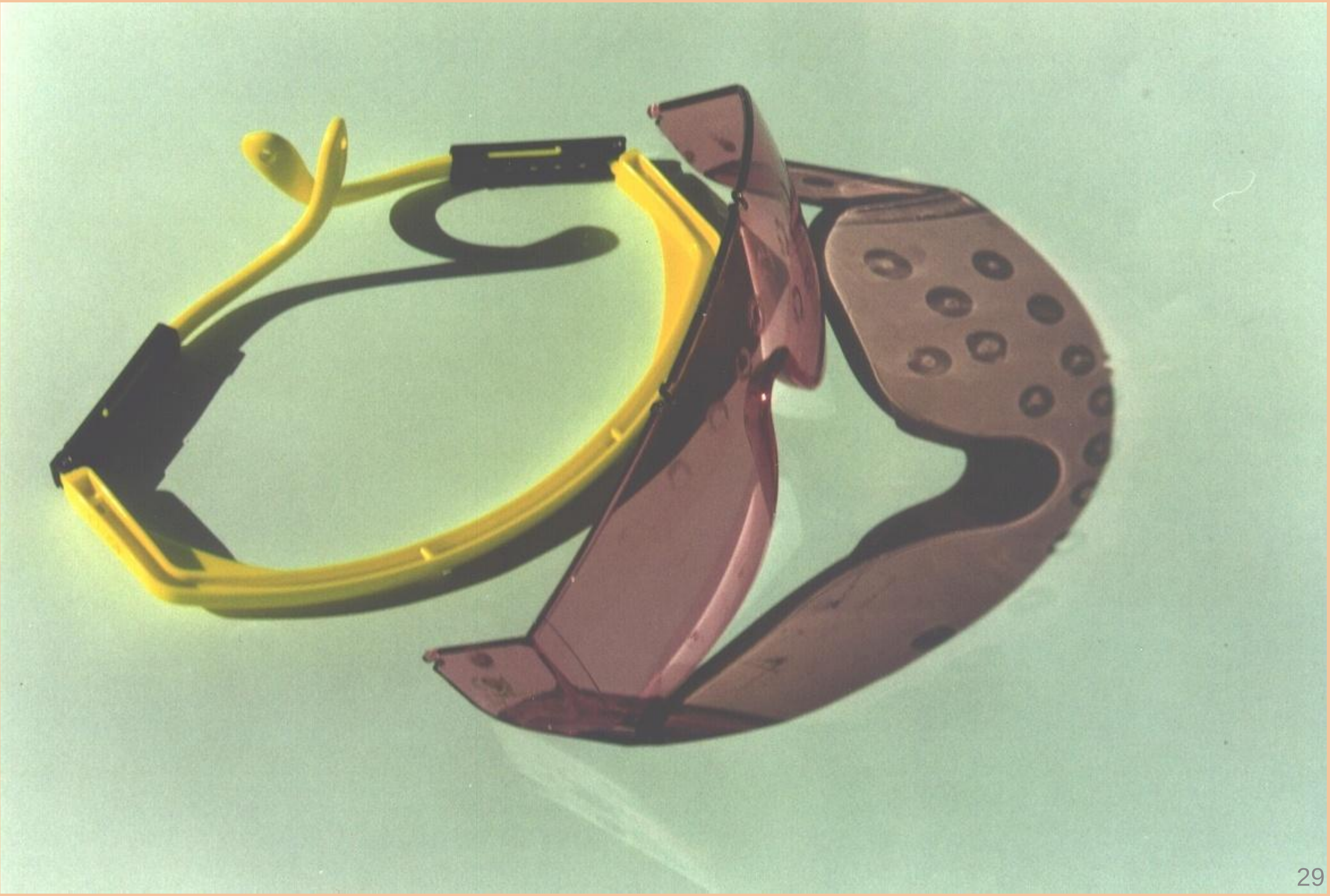

ESQUEMA EXPERIMENTAL

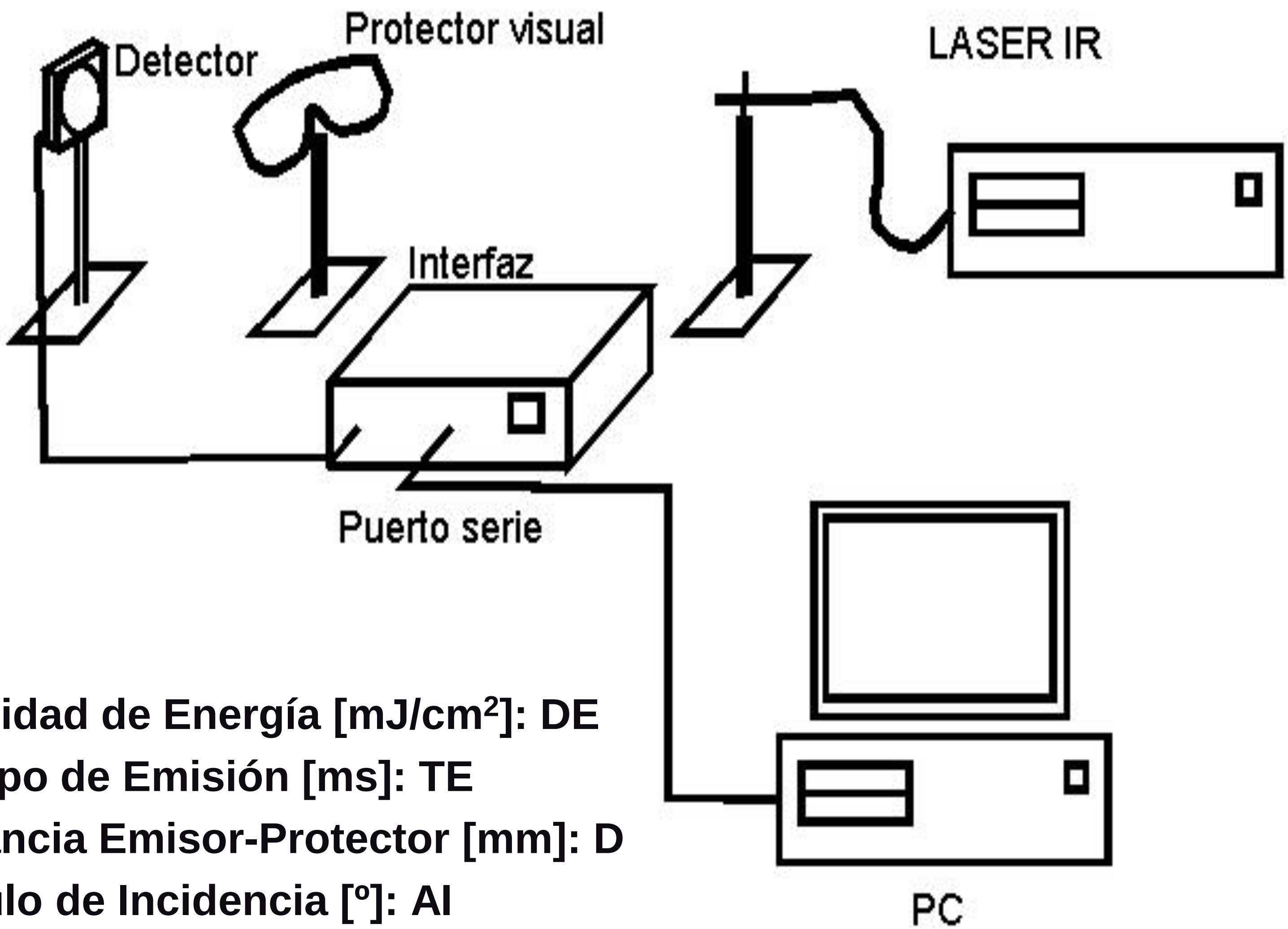

Densidad de Energía [mJ/cm^2]: DE

Tiempo de Emisión [ms]: TE

Distancia Emisor-Protector [mm]: D

Angulo de Incidencia [º]: AI

DISPOSICIÓN DE LAS IMPRONTAS I

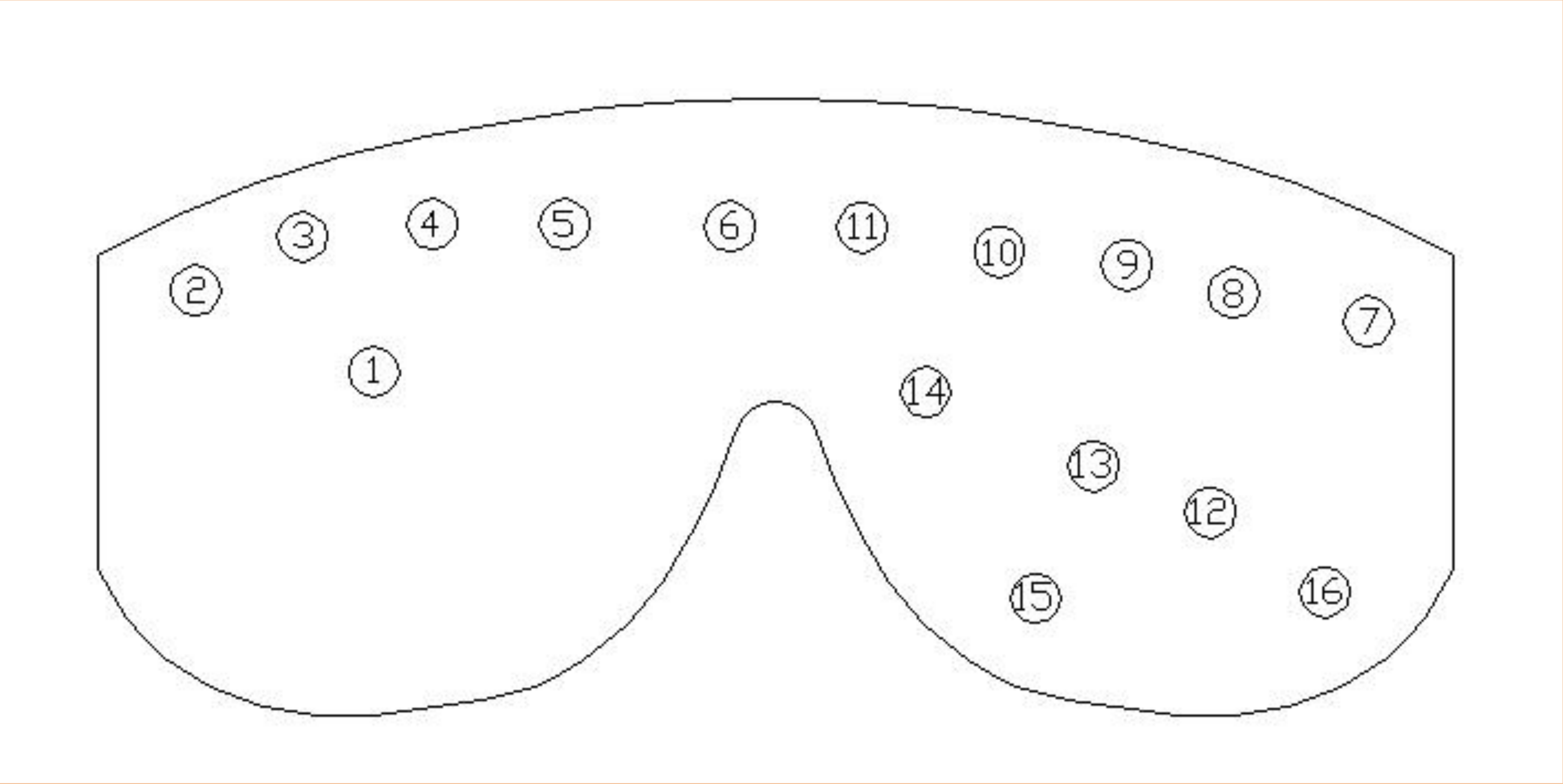

Impronta 1: Es la que produjo el accidente.
Improntas 2 a 16: Son las producidas para el estudio.

DISPOSICIÓN DE LAS IMPRONTAS II

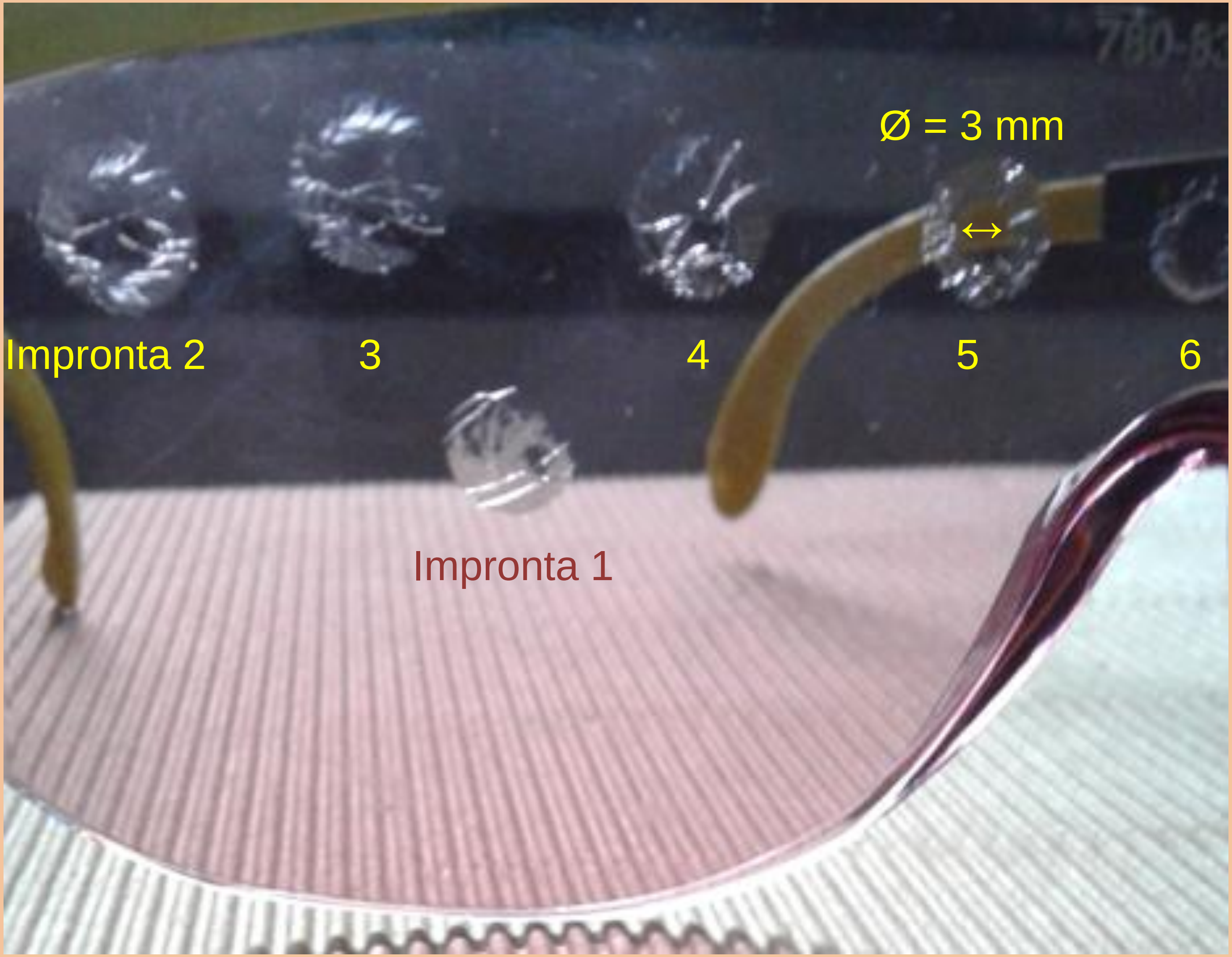

IMPRONTA 5

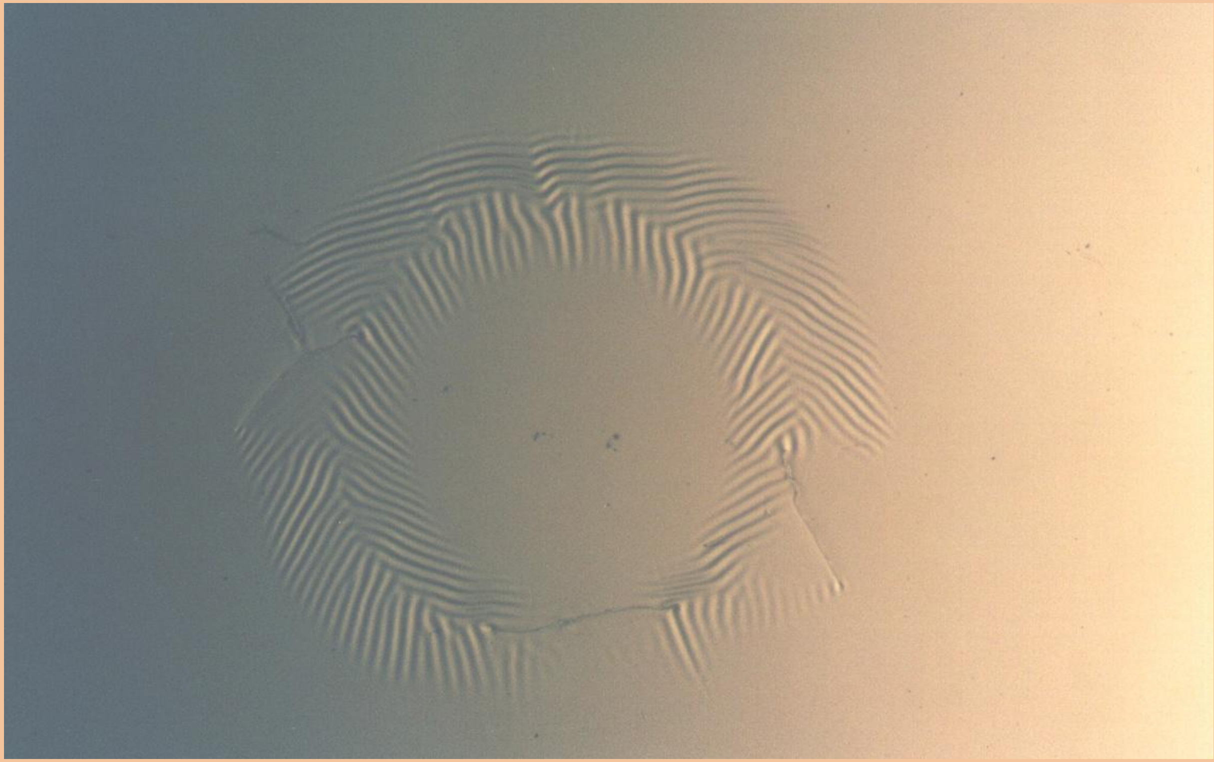

DE = 45 mJ/cm^2, TE = 250 ms, D = 75 mm, AI = 0º

IMPRONTA 9

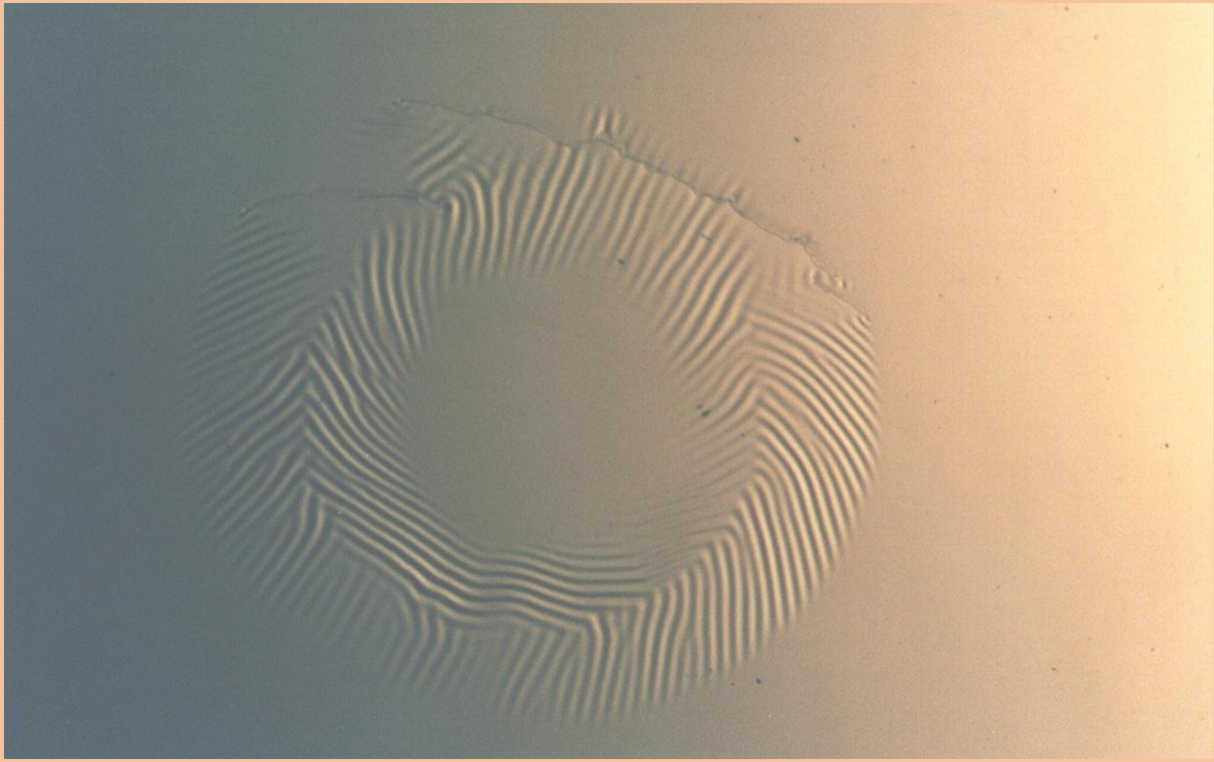

DE = 55 mJ/cm^2, TE = 250 ms, D = 75 mm, AI = 0º

IMPRONTA 13

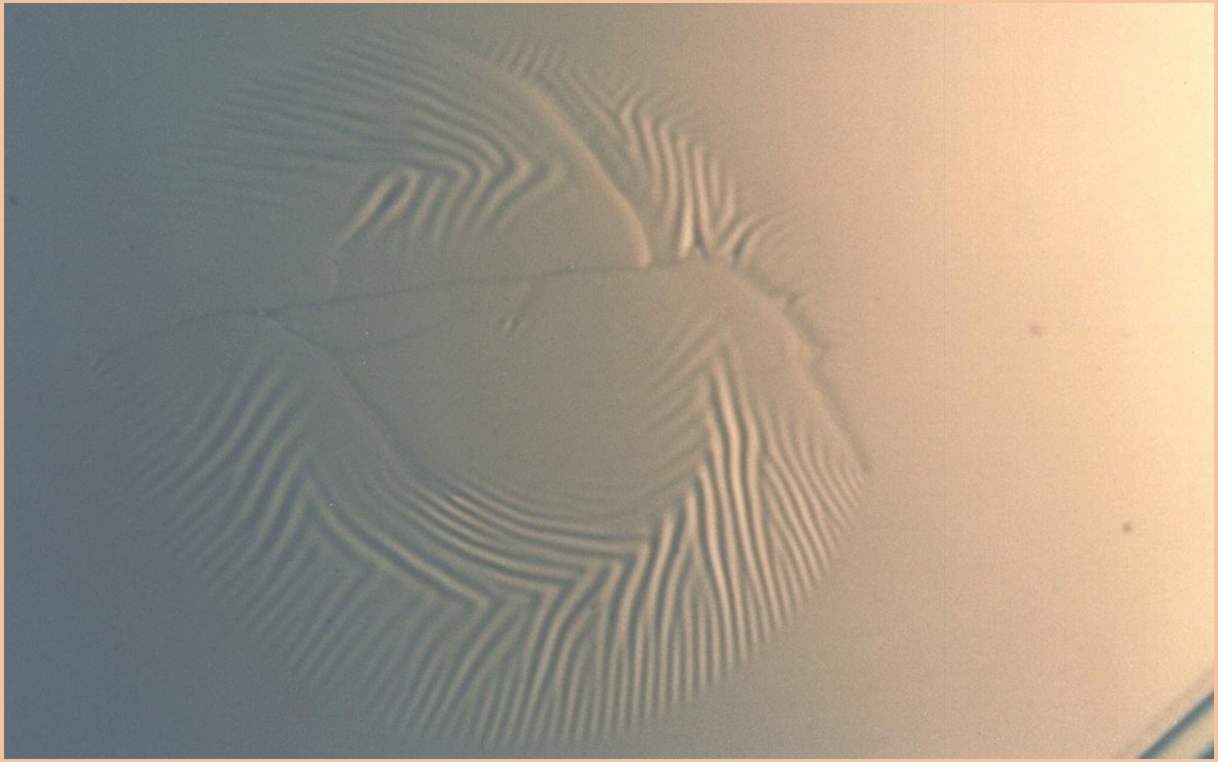

DE = 65 mJ/cm^2, TE = 250 ms, D = 75 mm, AI = 0º

IMPRONTA 16

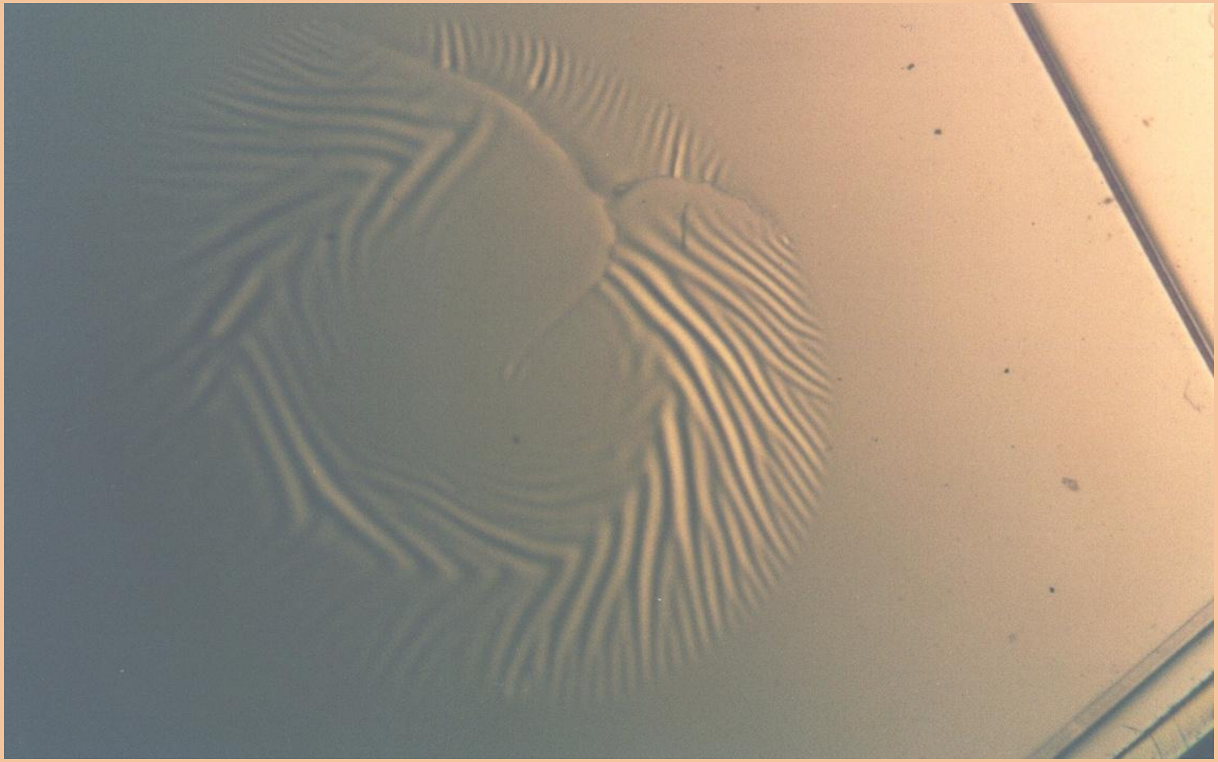

DE = 75 mJ/cm^2, TE = 250 ms, D = 75 mm, AI = 0º

TRANSMITANCIA SEGÚN EL PROVEEDOR PARA 810 nm

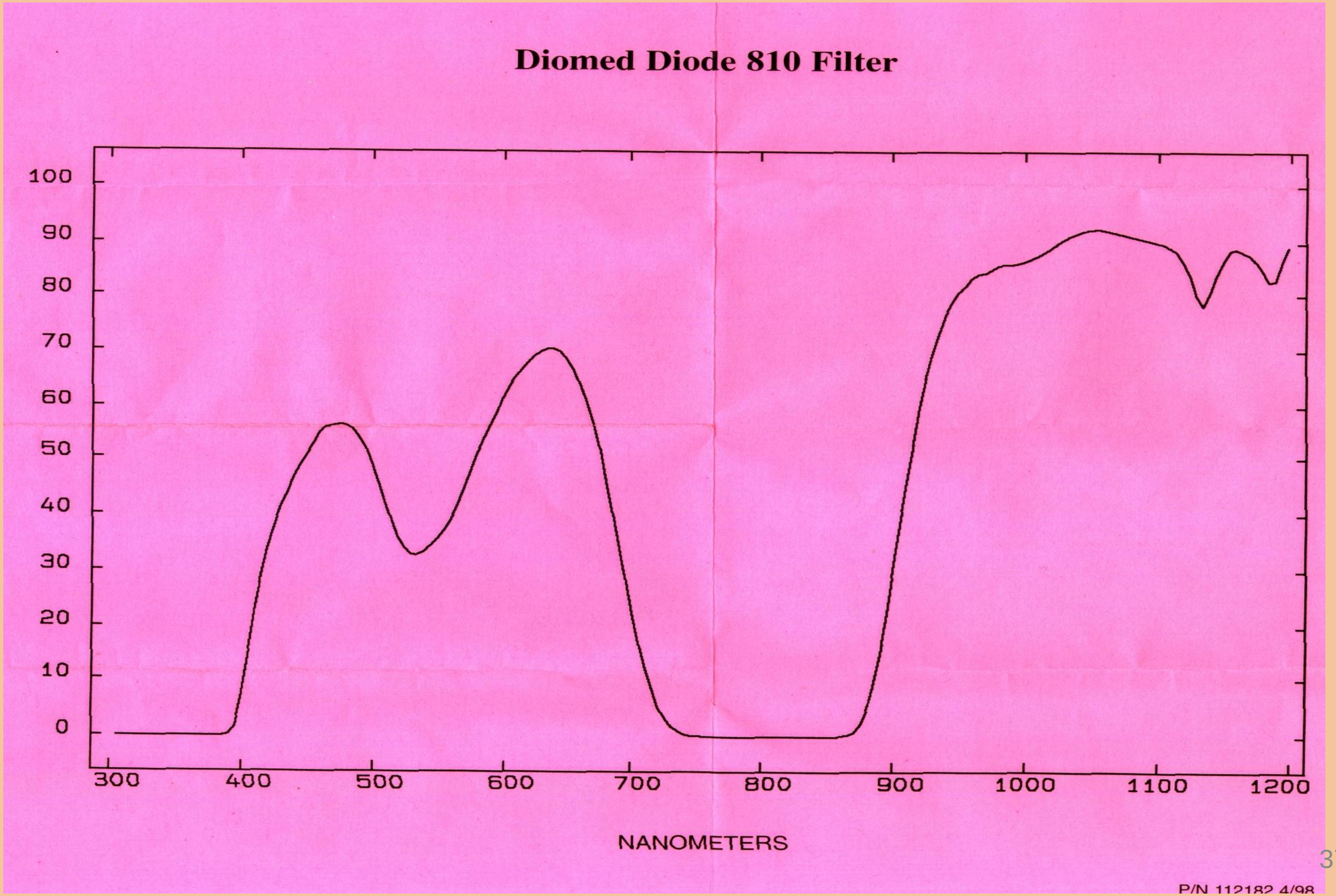

TRANSMITANCIA EN ZONA VIRGEN

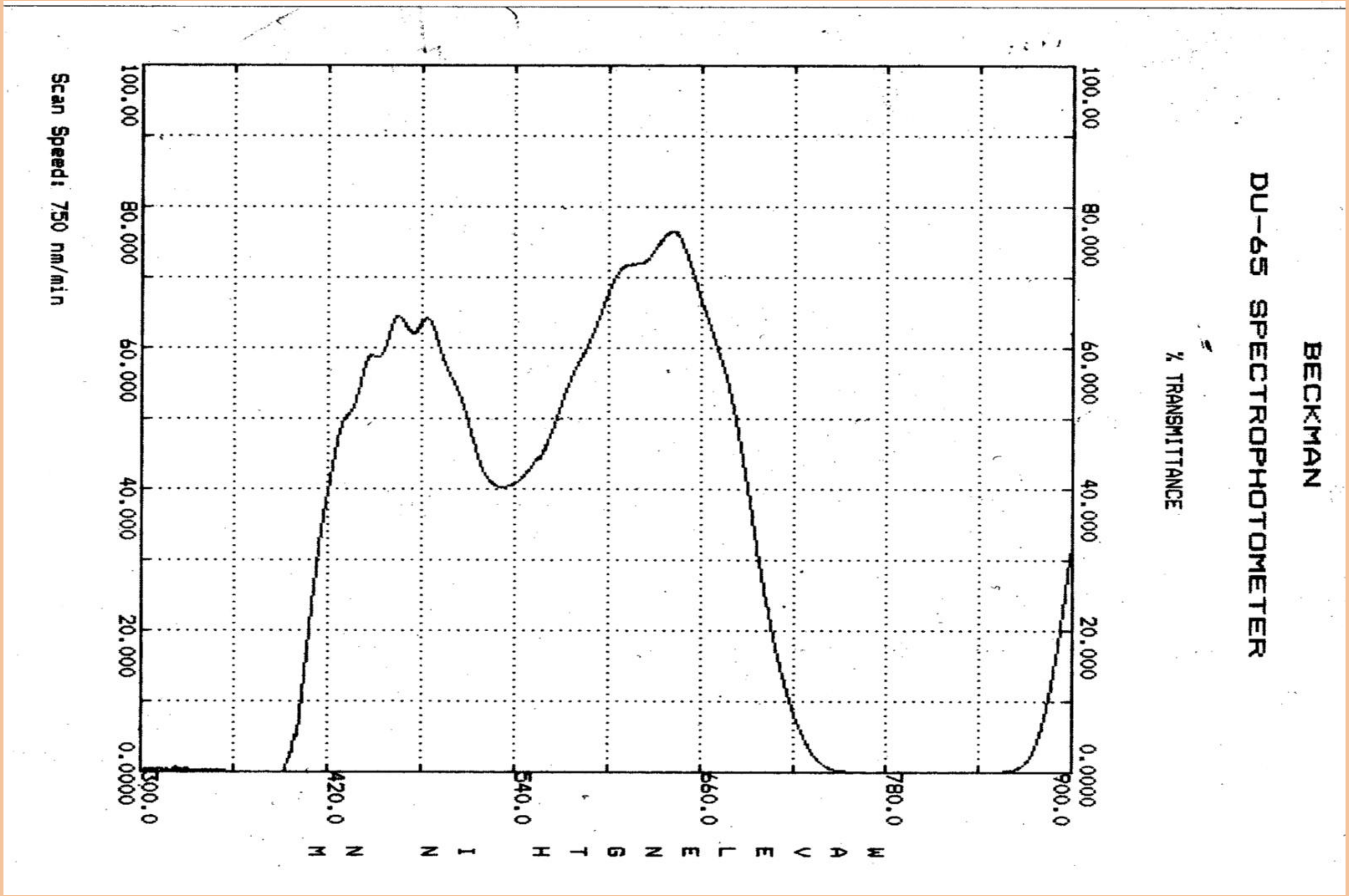

TRANSMITANCIA EN UN IMPACTO

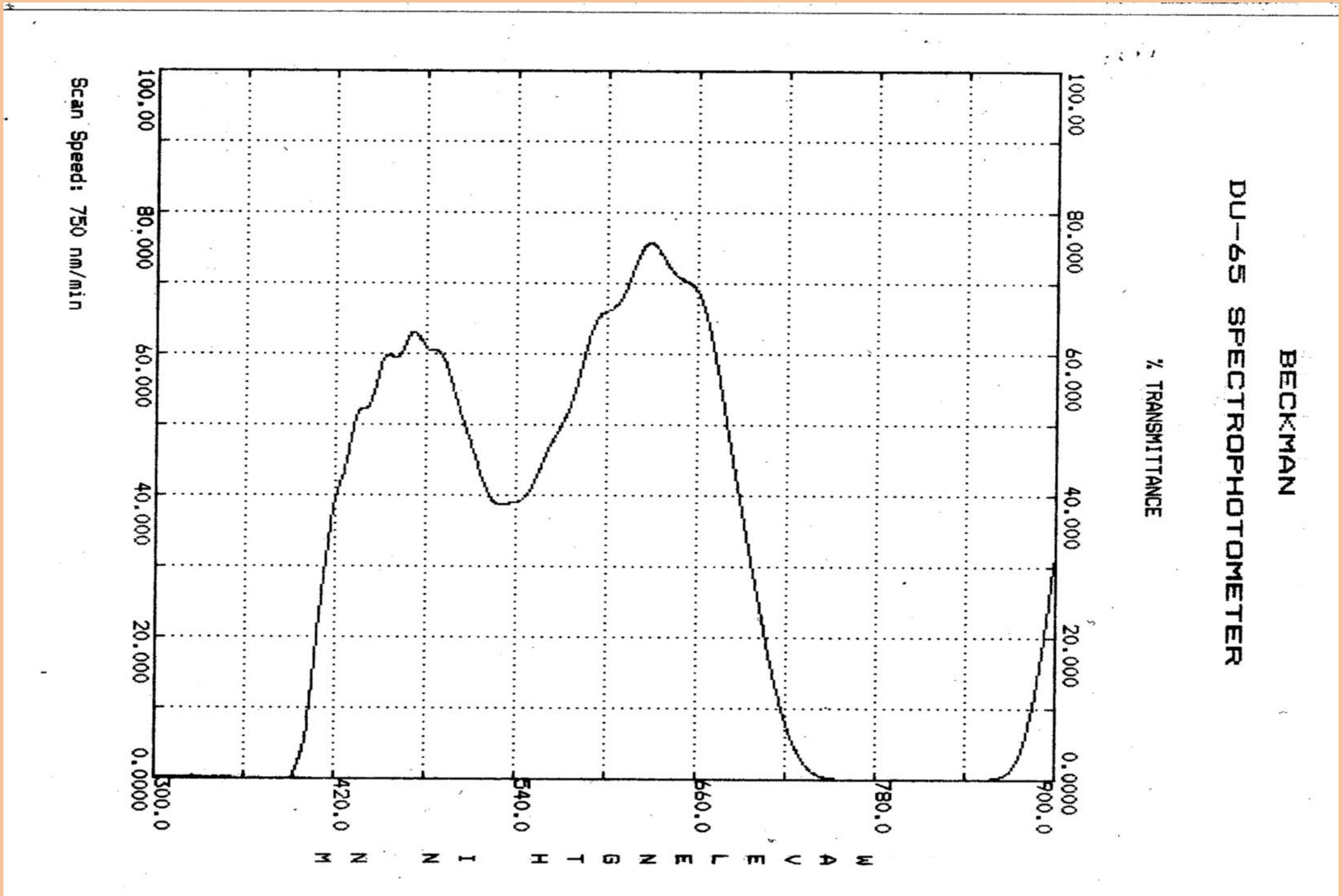

MEDICIONES DE TRANSMISIÓN DE ENERGÍA I

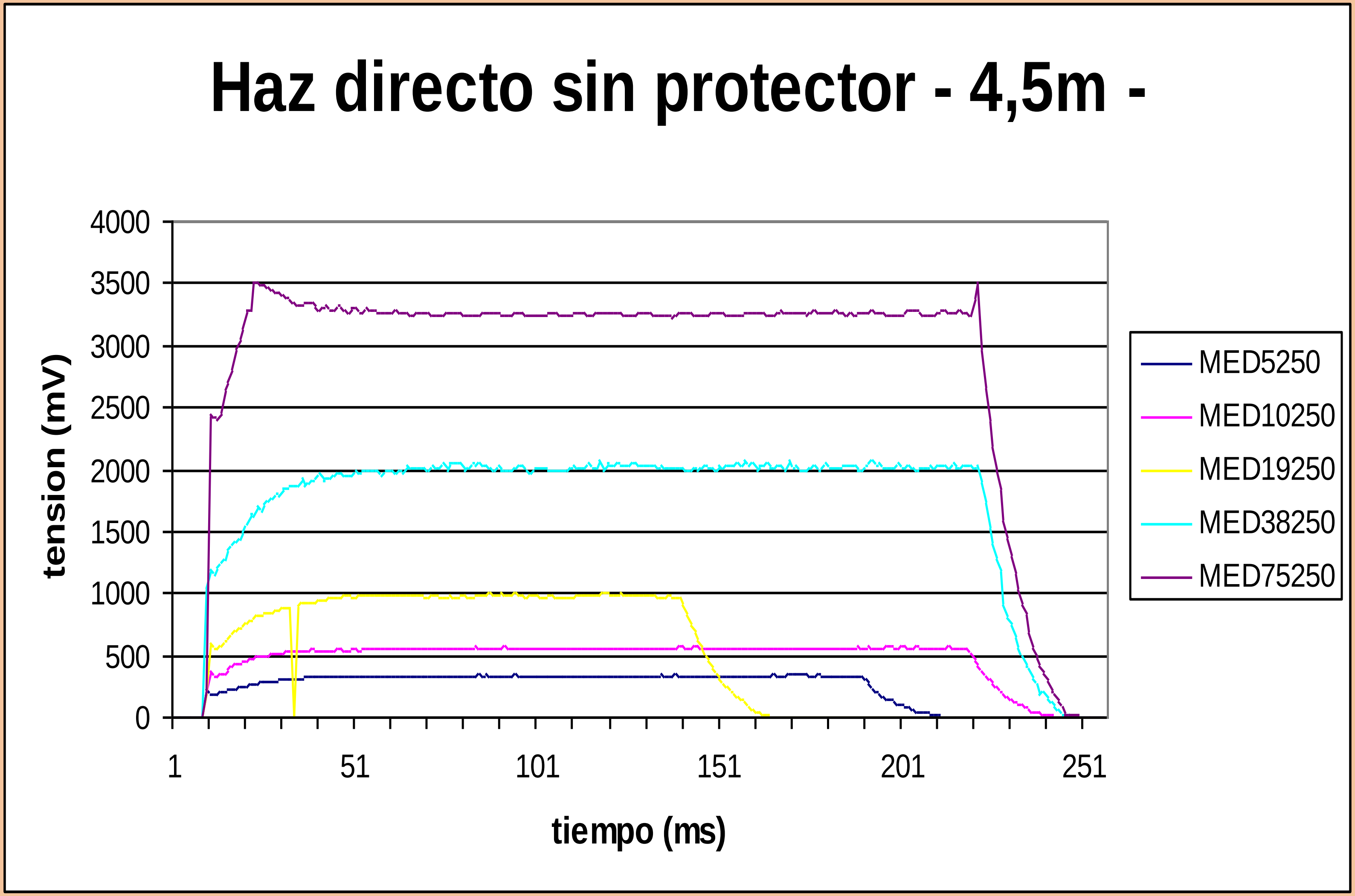

MEDICIONES DE TRANSMISIÓN DE ENERGÍA II

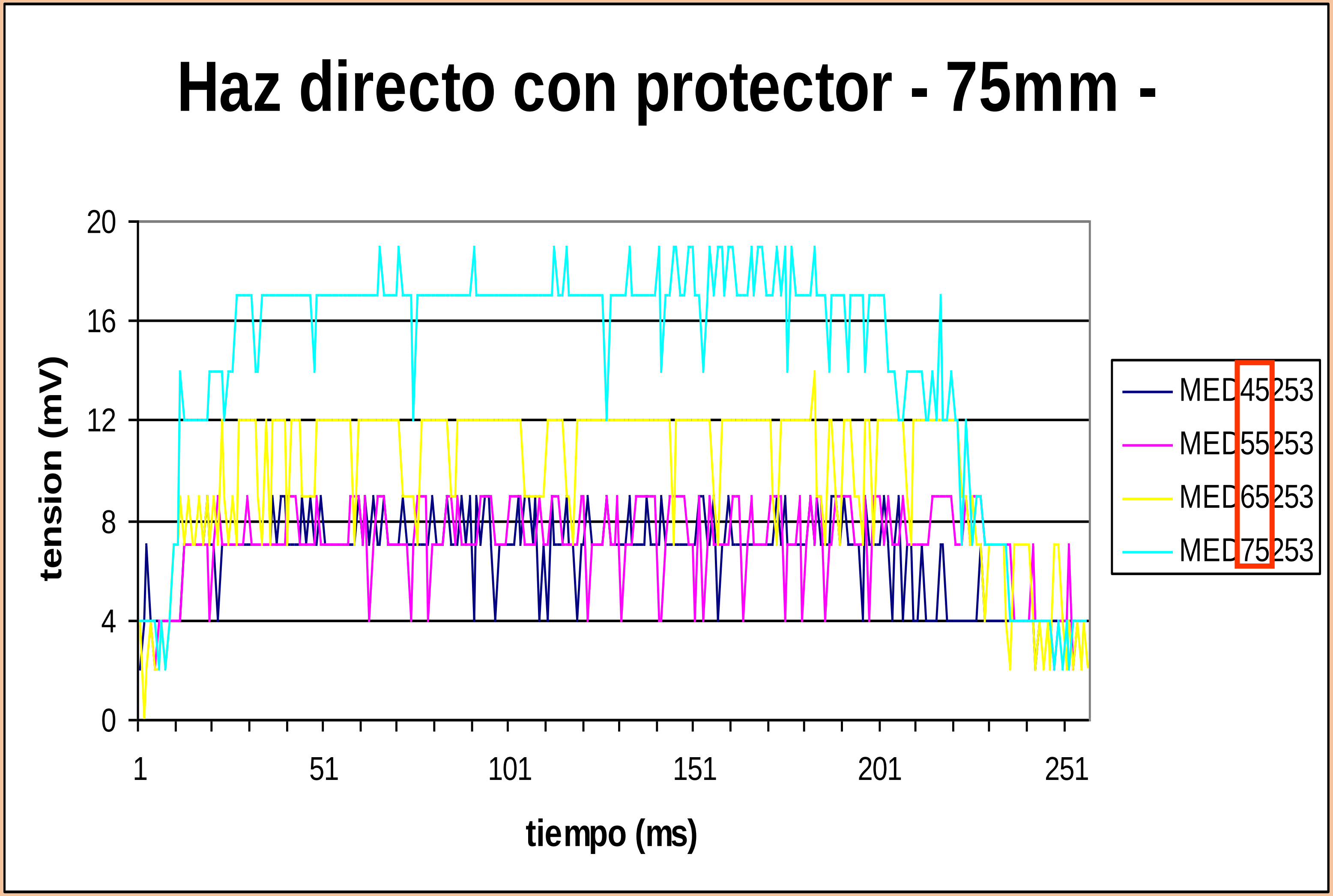

ANÁLISIS DE LOS DATOS

$\lambda_{\text{Fotón}}$ = 810 nm

$\nu_{\text{Fotón}}$ = 370,4 THz = 370,4 x 10^{12} Hz

$E_{\text{Fotón}} = h\nu_{\text{Fotón}} = 6{,}63 \times 10^{-34}$ J.s x 370,4 x 10^{12} Hz =

= 24,54 x 10^{-20} J

DE = 45 a 75 mJ/cm^2

Área de impacto, A = π x $0{,}15^2$ cm^2 = 0,07 cm^2

$E_{\text{Total mín.}}$ = 45 mJ/cm^2 x 0,07 cm^2 = 3,15 J

Fotones: $N_{\text{mín. Fotones}} = E_{\text{Total Máx.}} / E_{\text{Fotón}} = 2{,}14 \times 10^{16}$

GAFA PROTECTORA PARA LUZ LÁSER (Para λ = 810 nm, OD > 5)

Si DO > 5 → T < 0,000 001, significa, que de algo más de 1 000 000 fotones incidentes sobre la gafa no pasará ninguno, pero… ¡de 2,1 x 10^{16}!

CONCLUSIONES I

- Se produjeron improntas en el protector por incidencia de pulsos de radiación láser de 810 nm emitidos por el láser del accidente.
- Por espectrofotometría se obtuvieron las curvas de transmitancia de áreas vírgen del protector y otras afectadas por la irradiancia láser de elevada potencia pulsada. Tales curvas son parecidas y obtenidas según el modo de “baja señal”, sin perturbar al sistema observado.
- Se comparan dichas curvas con la entregada por el proveedor. Aparentan ser iguales.

CONCLUSIONES II

- Se diseñó un ensayo para estudiar los efectos de la incidencia pulsada de elevada irradiancia.
- El ensayo permitió verificar que, si bien el protector resiste incidencias directas –con atenuaciones algo menores que $1{:}10^{6}$ –, pero sin asegurar que pueda transmitir irradiancias significativas directas. **Sólo útil para luz láser difusa.**
- **Se recomienda incluir en los tests de los protectores para radiación láser los ensayos para incidencias pulsadas directas.**

Infrared Cholangiography in open surgery and its projection to minimally invasive surgery

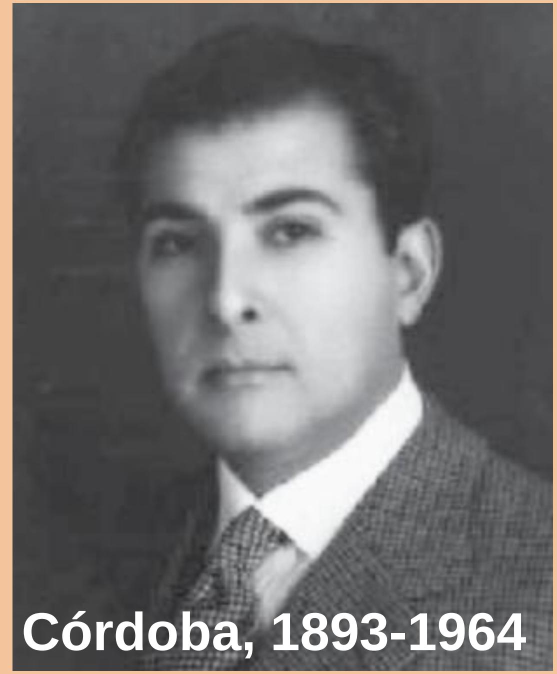

Desde que **Pablo Mirizzi** introdujo la **Intra-Operative Cholecystectomy** (**IOC**) empleando el Arco en C en los años 1930, su beneficio ha sido extensamente debatido. Nos propusimos reemplazar los **RX** por **Termografía IR**.

Each year, **over 750,000** patients undergo cholecystectomy in the **United States**, making it the most frequently performed abdominal surgical procedure. Common bile duct (**CBD**) injury during cholecystectomy occurs with relative infrequency (**1 in 200 to 400**) but ranks among the leading sources of **medical malpractice** claims against surgeons. Between **34% and 49%** of surgeons are expected to cause such an injury during their career. Repair of such injuries is often complex and requires multiple procedures. Major **CBD injury** also has a **substantial impact on quality of life, functional status, and survival.** **(2010 Report.)**
The **intra-operative Cholangiography** (I**OC)** is an **x-ray image** of the bile ducts produced after injection of a radiopaque contrast liquid during the Cholecystectomy, this procedure provides a map of the anatomy of the ducts in order to prevent CBD injury during the surgery. **Since Mirizzi [1] introduced IOC in the 1930's, its benefit has been extensively debated**. **Some surgeons advocate routine IOC use while others advise selective or no use**.

[1] **OPERATIVE CHOLANGIOGRAPHY.**
P. Mirizzi. Surg Gynecol Oncol 65:702–710. (1937)

Infrared Cholangiography in open surgery and its projection to minimally invasive surgery.

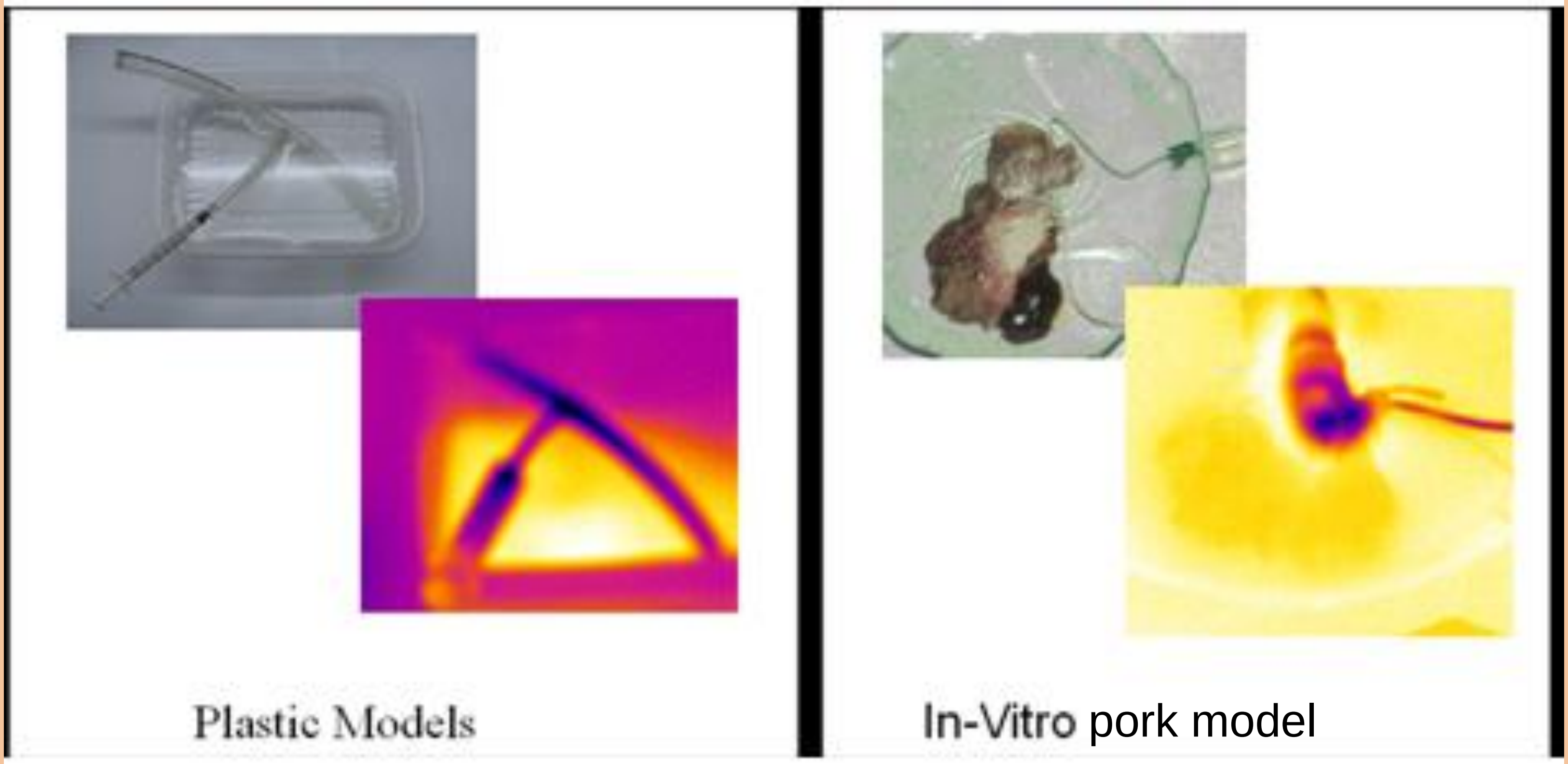

Infrared Cholangiography in open surgery and its projection to minimally invasive surgery.

P. Fluxa, C. Castilla, J.P. Rolland, and M. Garavaglia

Biomedical Optics Conferences, Optical Society of America, Florida, USA, 28 April to 2 May, 2012.

Infrared Cholangiography in open surgery and its projection to minimally invasive surgery.

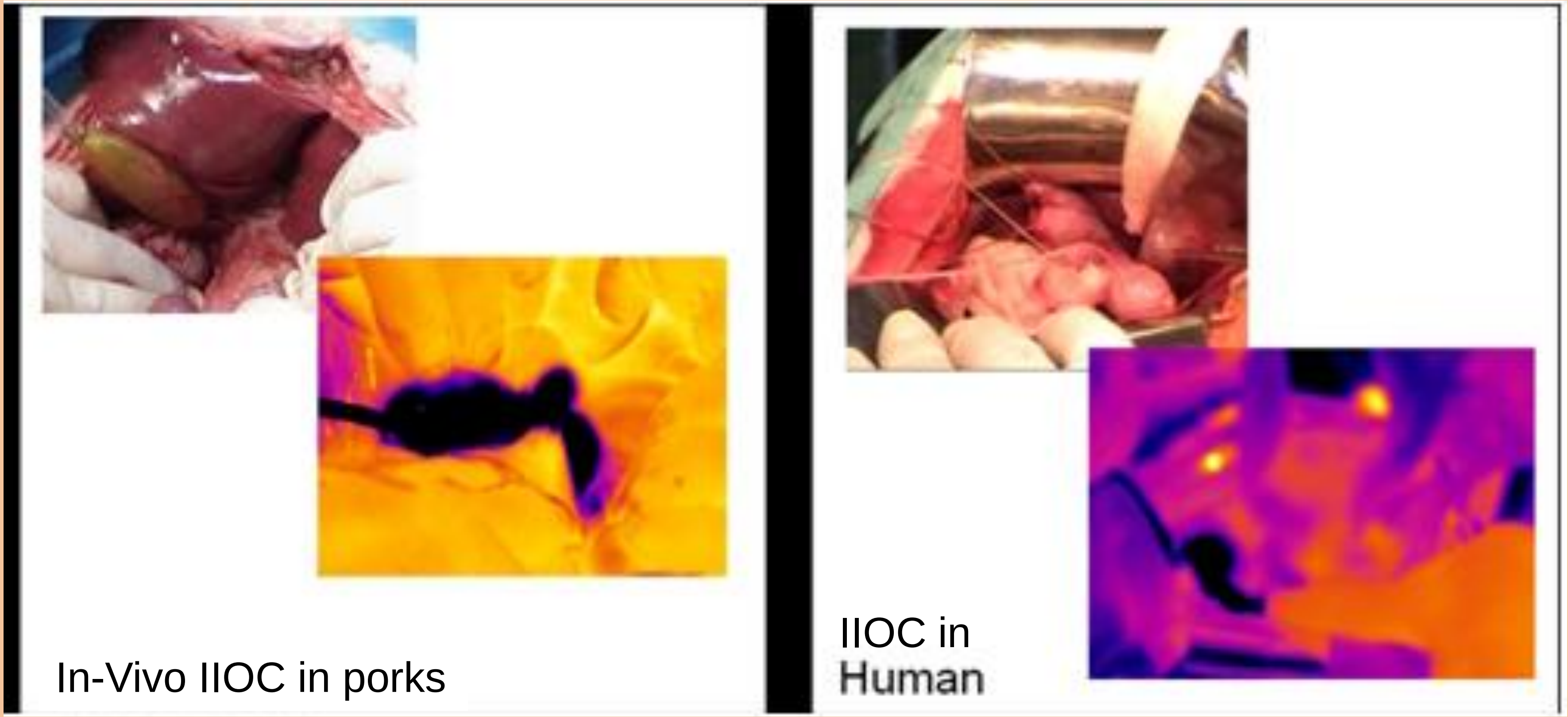

Infrared Cholangiography in open surgery and its projection to minimally invasive surgery.

P. Fluxa, C. Castilla, J.P. Rolland, and M. Garavaglia

Biomedical Optics Conferences, Optical Society of America, Florida, USA, 28 April to 2 May, 2012.

Infrared Cholangiography in open surgery and its projection to minimally invasive surgery.

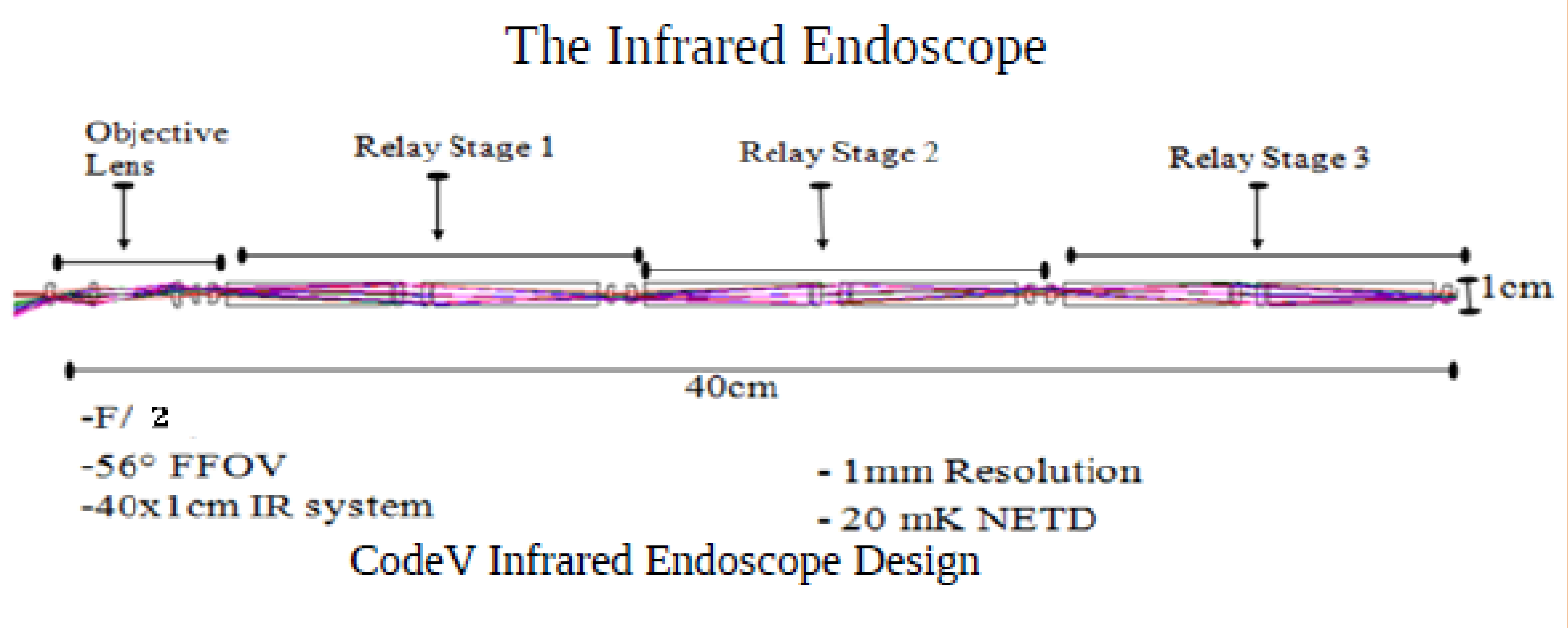

The optical design for the **IR endoscope** works in the **8-11μm range**. Lenses are made of Ge and AMTIR-1. The housing is made of stainless steel. The detector is a **640x480**, **17μm pixel pitch** uncooled microbolometer. The endoscope is an **F/2** system, with **1 mm resolution**.

Aplicación **biomédica** de la tomografía por ondas de 0,3 a 10 **THz** (λ = 30 mm a 1 mm)

La publicación:

Review of Terahertz Tomography Techniques.
Jean Paul Guillet, Benoît Recur, Louis Frederique, Bruno Bousquet, Lionel Canioni, Inka Manek-Hönninger, Pascal Desbarats, and Patrick Mounaix
J. of IR, mm and THz Waves, Springer, **2014**, 35, 382-411.

Sólo menciona estas publicaciones en Biomedicina:

1. Fitzgerald, A.J., et al. Catalogue of human tissue optical properties at terahertz frequencies. Journal of Biological Physics, **2003**. 29(2-3): 123-128.

2. Fitzgerald, A.J., et al. Terahertz pulsed imaging of human breast tumors. Radiology, **2006**. 239(2): 533-540.

3. Nakajima, S., et al. Terahertz imaging diagnostics of cancer tissues with a chemometrics technique. Applied Physics Letters, **2007**. 90(4): 041102.

Aplicación **biomédica** de la tomografía por ondas de 0,3 a 10 **THz** (λ = 30 mm a 1 mm)

4. Watanabe, Y., et al. Component spatial pattern analysis of chemicals using terahertz spectroscopic imaging. Applied Physics Letters, **2003**. 83(4): 800-802.

5. Beard, M.C., et al. Progress towards two-dimensional biomedical imaging with THz spectroscopy. Physics in Medicine and Biology, **2002**. 47(21): 3841-3846.

6. Crowe, T.W., et al. Terahertz sources and detectors and their application to biological sensing. Philosophical Transactions of the Royal Society of London Series a-Mathematical Physical and Engineering Sciences, **2004**. 362(1815): 365-374.

7. Stringer, M.R., et al. The analysis of human cortical bone by terahertz time-domain spectroscopy. Physics in Medicine and Biology, **2005**. 50(14): 3211-3219.

INTERACTION OF TERAHERTZ RADIATION WITH DNA

A. N. Bugay. Joint Institute for Nuclear Research, Dubna, Russia. Nanosystems: Physics, Chemistry, Mathematics, **2012**, 3 (1), P. 51–55

“The importance of proton tunneling in chemical and biological systems is well known for the DNA base pairing and mutagenesis. The proton can tunnel into less energy favorable tautomer state of base pair, which may cause incorrect pairing during DNA replication. There are a lot of theoretical studies of proton tunneling in such systems. It is demonstrated that terahertz radiation (**0.1-10 THz**) can induce conformational changes in proteins and nucleic acids, and also **can influence the number of spontaneous and induced point mutations**. These **preliminary theoretical results** can qualitatively explain the **results of experimental observations of terahertz influence on the number of spontaneous and induced point mutations**.”

Passive THz imaging may be an alternative to controversial **airport body scanners**. I

Torsten May, **Hans-Georg Meyer** and **Jürgen Popp**. SPIE Defense, Security, and Sensing Conferences. SPIE Photonics Europe. April 2010.

In recent years, body scanner technologies based on X-ray or millimeter waves (**MMW**) have been shown to improve security in areas sensitive to terroristic attacks such as airports. However, even if the need for such measures is evident, **such technologies raise health and privacy concerns**, especially since the body-scanners recently installed in airports in Europe, the United States, and elsewhere see through clothing and reveal clear **outlines of passengers' anatomies**. Although these scanning technologies are said to be harmless, a residual risk remains, according to a recent study on **genotoxic effects** of active MMW body-scanner radiation. Therefore, a high-level security tool which eliminates the health concerns and addresses privacy issues would be highly beneficial.

… see through clothing and reveal clear outlines of passengers' anatomies.

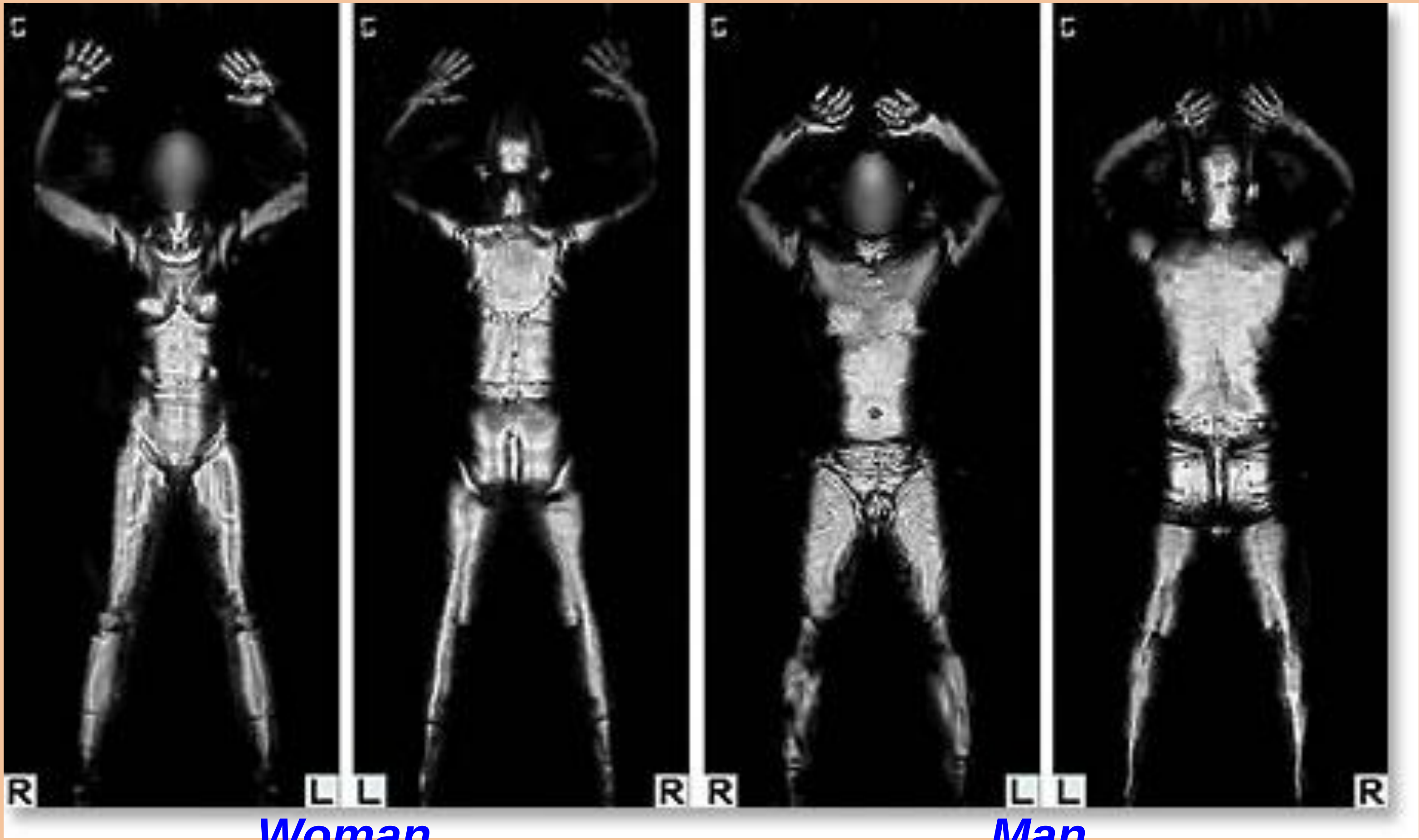

Woman **Man**

Millimeter wave technology produces whole body images that reveal outlines of a person's anatomy as well as concealed objects such as weapons and explosives.

ATENUACIÓN DE ONDAS EM

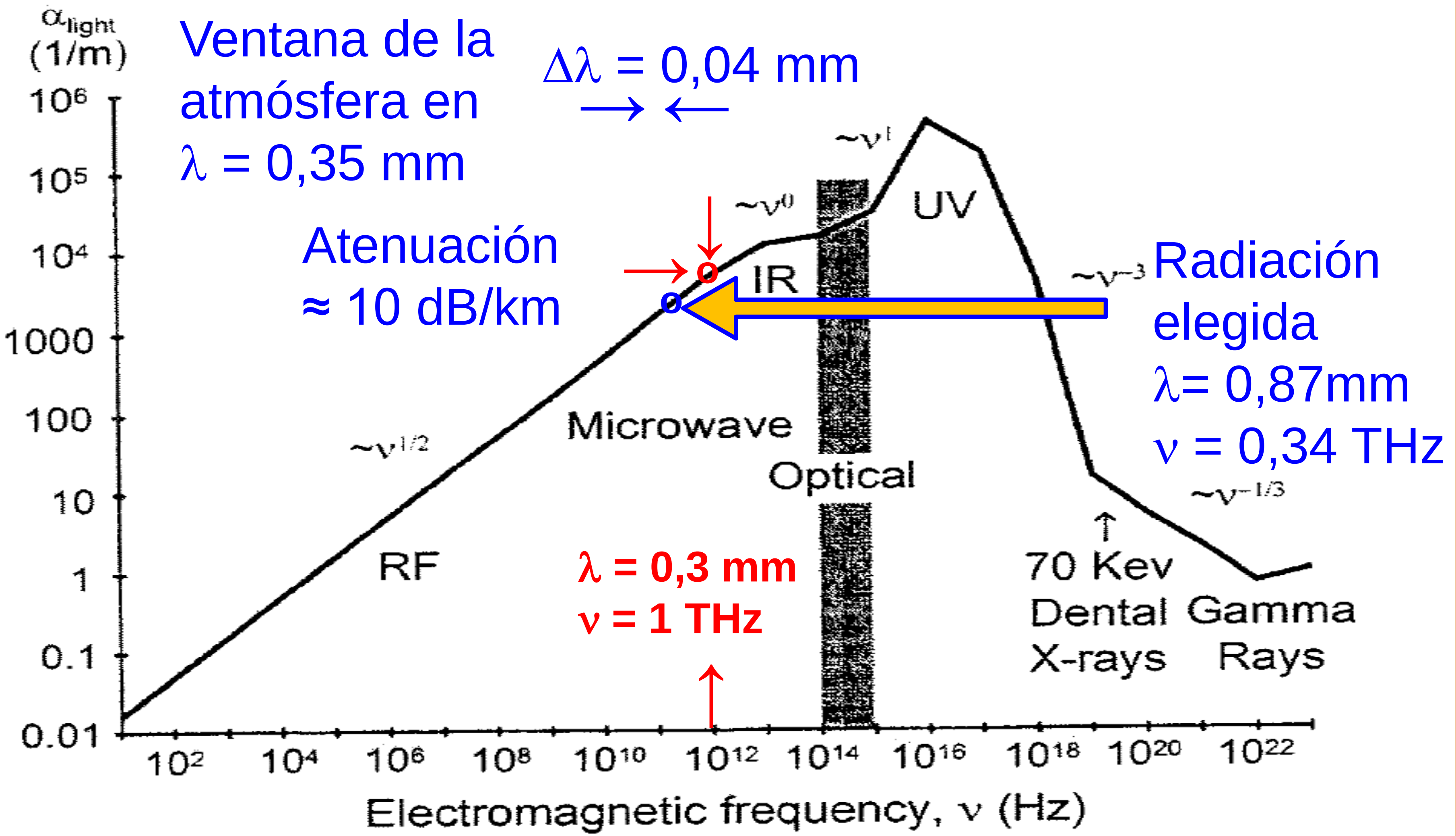

Fig. 12.41. Attenuation of electromagnetic radiation in human tissue, due to absorption and scattering. (From [576]. Courtesy of Robert A. Freitas Jr., Nanomedicine, Vol. 1 (1999), http://www.nanomedicine.com)

Passive THz imaging may be an alternative to controversial **airport body scanners**. II

Candid Cameras

The demonstrator built at the Institute of Photonic Technology (Jena, Germany) uses Cassegrain-type reflective optics with a **50-cm aperture**, allowing for a spatial resolution of about **1 cm** at a distance of **5 m**. It was possible to construct a **sub-THz camera** that visualizes a **person's body heat**. However, because of the large corresponding wavelength (**870 µm**), the **diffraction**-limited spatial resolution is an issue which requires the use of **sizable optics**.

RECEPCIÓN PASIVA EN LA BANDA DE 0,34 THz

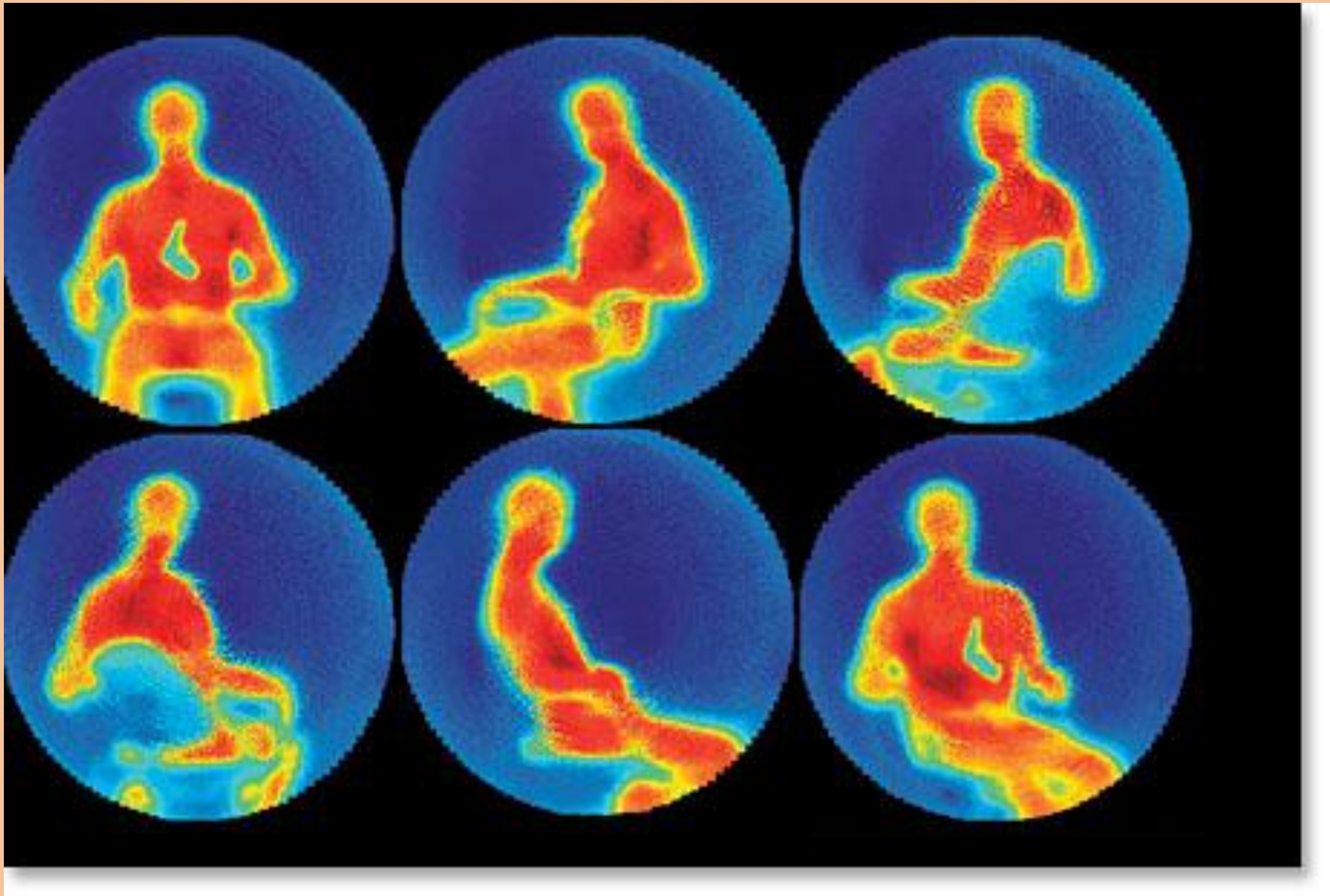

Freeze images from a movie with a 4-Hz frame rate show a person sitting on a lab chair. A handgun mock-up is hidden under clothing, in upper left and lower right.

Laser-Compton X-ray and γ-ray I

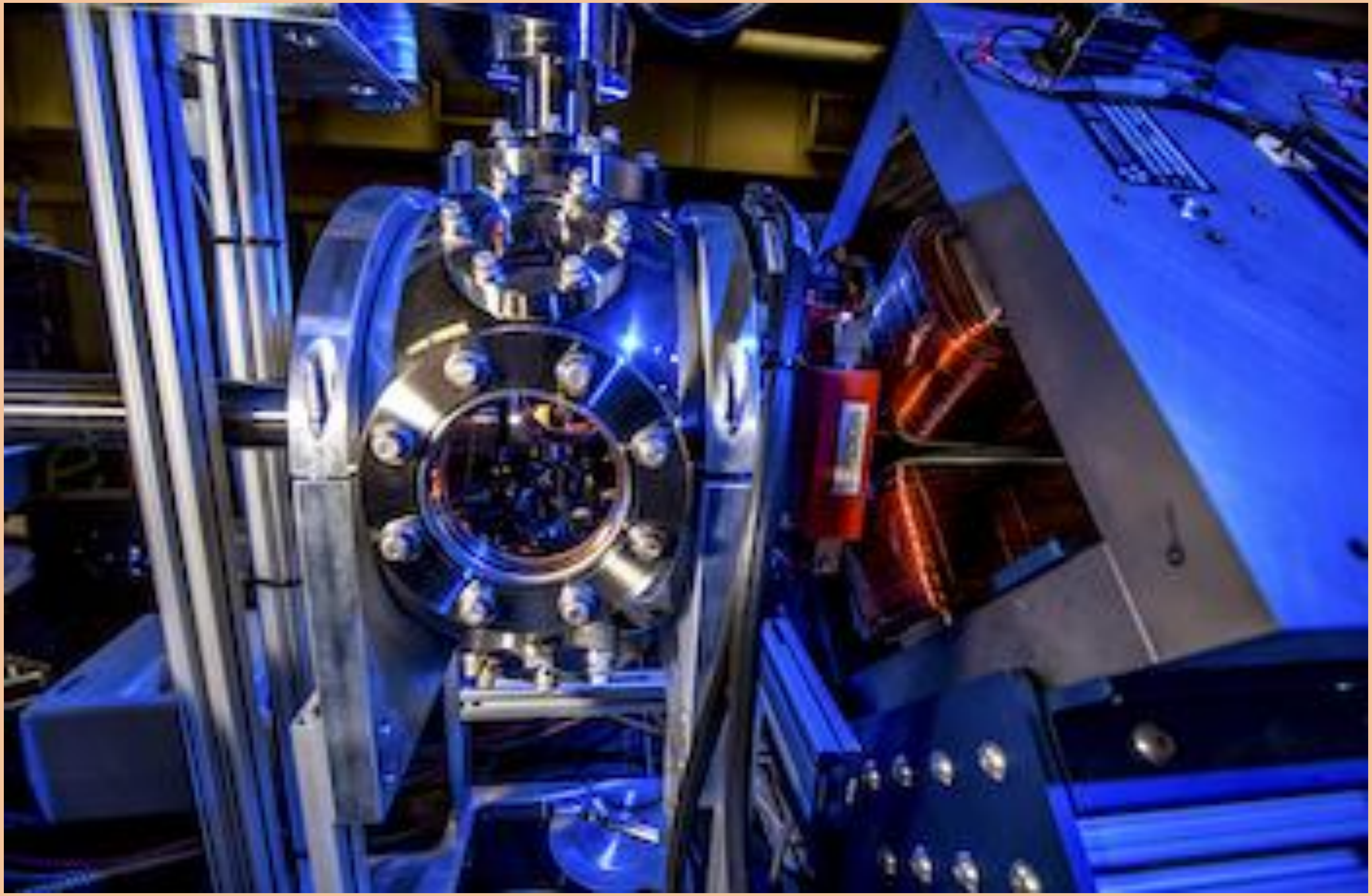

X-ray (Not atomical) and γ-ray (Not nuclear) source: Where electrons and laser beam collide.

Laser-Compton X-ray and γ-ray II

As honed at **Lawrence Livermore National Laboratory** (LLNL) over the last decade, **Laser-Compton light source technology** produces **mono-energetic gamma rays** and **X-rays through the collision of an electron beam and a laser beam**. According to **LLNL**, the peak brightness of a **Laser-Compton light source** pulse can be **15 orders of magnitude** beyond any other man-made light, in the million-electron-volt (**MeV**) spectral range.

Laser-Compton X-ray I

Conventional **clinical X-ray systems** operate on principles similar to the original technology demonstrated by **Wilhelm Röntgen**, in which a beam of energetic electrons is focused onto a metal anode to create the X-rays. The resolution of the resulting shadowgraphs depends on the electron spot size, typically greater than **500 microns**, with an **effective X-ray spot size of around 600 to 800 microns**.

Laser-Compton X-ray II

"In a laser-Compton source, the **effective X-ray spot size is set by the focal spot size of the laser** used in the collision with the electron beam, and in principle can be of the **same order as the wavelength of the light**," said Professor **Chris Barty**, IP of the **Lumitron** project. "Since the monochromatic nature of on-axis radiation from a laser-Compton source is compatible with standard X-ray optical systems, combining a laser-Compton source with appropriate X-ray optics should allow creation of **effective X-ray spot sizes of around 100 nanometers**."

Laser-Compton X-ray III

Lumitron is based at the **University of California**, **Irvine**, (UCI) a location offering synergy with the Beckman Laser Institute and UCI Applied Innovation, and intends to develop laser-Compton light sources with monochromatic **100 keV-class X-ray** outputs comparable to those from large-scale synchrotrons. The nature of these X-rays should allow both **enhanced resolution** in the resulting shadowgraphs and **significant reductions in dosage**, compared to current imaging and therapeutic modalities. One significant development enabling the **Laser-Compton** concept to be made more compact and operate at high flux, both important for clinical settings.

Laser-Compton X-ray IV

HyperVIEW platform promises cellular-level imaging and treatment

¡LES AGRADEZCO LA COMPAÑÍA!